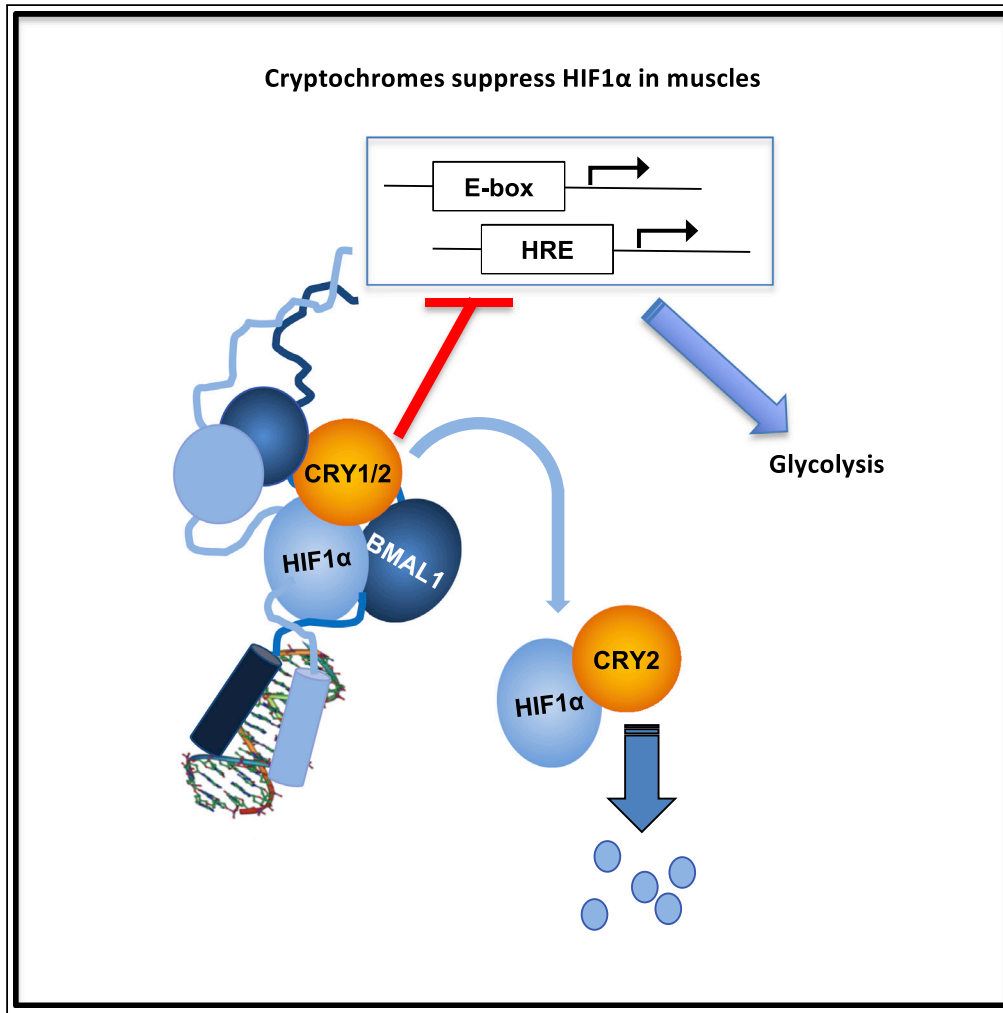


Article

Cryptochromes Suppress HIF1 α in Muscles



Megan E. Vaughan, Martina Wallace, Michal K. Handzlik, Alanna B. Chan, Christian M. Metallo, Katja A. Lamia

klamia@scripps.edu

HIGHLIGHTS

CRY2 plays a unique role in regulating HIF1 α protein accumulation in muscle

HIF1 α and BMAL1 heterodimers are transcriptionally active

CRY1/2 represses transcription driven by HIF1 α /BMAL1 heterodimers

Cryptochromes influence skeletal muscle substrate preference and utilization

Vaughan et al., iScience 23, 101338
July 24, 2020 © 2020 The Authors.
<https://doi.org/10.1016/j.isci.2020.101338>



Article

Cryptochromes Suppress HIF1 α in Muscles

Megan E. Vaughan,¹ Martina Wallace,² Michal K. Handzlik,² Alanna B. Chan,¹ Christian M. Metallo,² and Katja A. Lamia^{1,3,*}

SUMMARY

Muscles preferentially utilize glycolytic or oxidative metabolism depending on the intensity of physical activity. Transcripts required for carbohydrate and lipid metabolism undergo circadian oscillations of expression in muscles, and both exercise capacity and the metabolic response to exercise are influenced by time of day. The circadian repressors CRY1 and CRY2 repress peroxisome proliferator-activated receptor delta (PPAR δ), a major driver of oxidative metabolism and exercise endurance. CRY-deficient mice exhibit enhanced PPAR δ activation and greater maximum speed when running on a treadmill but no increase in exercise endurance. Here we demonstrate that CRYs limit hypoxia-responsive transcription via repression of HIF1 α -BMAL1 heterodimers. Furthermore, CRY2 appeared to be more effective than CRY1 in the reduction of HIF1 α protein steady-state levels in primary myotubes and quadriceps *in vivo*. Finally, CRY-deficient myotubes exhibit metabolic alterations consistent with cryptochrome-dependent suppression of HIF1 α , which likely contributes to circadian modulation of muscle metabolism.

INTRODUCTION

Tissue hypoxia results from an imbalance between local oxygen consumption and the ability of associated vasculature to replenish oxygen. Hypoxia has long been studied in the context of cancer, with the observation that cancerous cells residing deep within solid tumors are exposed to an oxygen-poor local microenvironment. Cancer cells preferentially produce energy through glycolysis rather than oxidative phosphorylation, which allows them to survive in hypoxic environments and provides additional growth advantages that are as yet incompletely understood (Liberti and Locasale, 2016). In normal physiology, the hypoxia signaling network is an adaptive response designed to accommodate the immediate metabolic demands of a tissue and facilitate long-term adaptation to inadequate oxygen levels (Hoppeler and Vogt, 2001). This is particularly important in skeletal muscle, which must adapt to rapid and dramatic fluctuations in mean oxygen tension during strenuous exercise. Activation of hypoxic signaling in muscles stimulates both an immediate shift to glycolytic flux and long-term adaptations such as increased vascularization (Lindholm and Rundqvist, 2016). Mice with genetically attenuated hypoxia signaling in skeletal muscles exhibit enhanced reliance on oxidative phosphorylation for energy production. When sedentary, they have greater low-intensity exercise endurance. However, they are more susceptible to muscle damage; after training, they exhibit lower endurance capacity than wild-type (WT) controls (Mason et al., 2004).

Much of the hypoxic signaling cascade in mammals is activated via a group of transcription factors known as hypoxia-inducible factors (HIFs), which are part of the larger bHLH-PAS domain family of DNA-binding proteins (Dengler et al., 2014). These proteins are canonically composed of two subunits that heterodimerize and activate transcription of target genes via hypoxia response elements (HREs). This heterodimer pair is composed of the oxygen-sensitive HIF1 α and the constitutively expressed HIF1 β subunits. Regulation of hypoxic signaling involves the integration of numerous metabolic signals, including components of the MAPK pathway, citric acid cycle intermediates, and reactive oxygen species (ROS) (Bardos and Ashcroft, 2005). Most directly implicated in regulation of HIF1 α /HIF1 β signaling, however, are the class of enzymes known as prolyl hydroxylases (PHDs), which in mammals are encoded by the genes *EGLN1-3*. When oxygen is readily available, HIF1 α is rapidly hydroxylated by PHDs on two prolines within its oxygen-dependent degradation domain, leading to its association with the von Hippel-Lindau (vHL) E3 ubiquitin ligase and subsequent degradation by the proteasome (Ivan and Kaelin, 2017). These PHD enzymes are 2-oxoglutarate (also known as alpha ketoglutarate, α KG)-dependent dioxygenases that rely on molecular oxygen,

¹Department of Molecular Medicine, Scripps Research, La Jolla, CA 92037, USA

²Department of Bioengineering, University of California, San Diego, La Jolla, CA 92093, USA

³Lead Contact

*Correspondence: klamia@scripps.edu

<https://doi.org/10.1016/j.isci.2020.101338>



α KG, vitamin C, and iron as cofactors for their function. As such, PHD enzymes are inhibited under conditions of hypoxia or upon exposure to iron chelators or small molecules that displace α KG (Tian et al., 2011; Yuan et al., 2003). This leads to stabilization of HIF1 α , which heterodimerizes with HIF1 β to activate target genes containing one or more HRE sequences within their promoters (Ivan and Kaelin, 2017).

Like HIFs, the circadian clock is highly regulated and sensitive to modulation by metabolic signals. In mammals, circadian oscillators are composed of a transcription/translation feedback loop, in which the bHLH-PAS transcription factors CLOCK and BMAL1 activate the transcription of numerous clock-controlled genes, including their own repressors, period (PER1/2/3) and cryptochrome (CRY1/2) (Takahashi, 2017). HIF1 α , HIF1 β (also known as ARNT), CLOCK, and BMAL1 all belong to the bHLH-PAS family (Wu and Rastinejad, 2017) and can form heterodimeric pairs via their highly conserved bHLH domains (Fribourgh and Partch, 2017). HIF1 α and BMAL1 can directly interact in yeast two-hybrid assays (Hogenesch et al., 1998) and can associate in mammalian cells (Wu et al., 2017). Furthermore, genetic deletion of *Bmal1* prevents hypoxia-induced recruitment of HIF1 α to a significant fraction of its binding sites in chromatin (Wu et al., 2017). Although these prior findings support a role for BMAL1-HIF1 α heterodimers in a subset of hypoxia responses, the extent of this interaction under normal physiological conditions and its implications for circadian and hypoxia-responsive transcriptional networks are not well understood.

It was recently demonstrated that HIF1 α is involved in the regulation of circadian clock. Mice subjected to mildly reduced atmospheric oxygen were reported to exhibit HIF1 α -dependent accelerated adaptation to a change in lighting conditions that mimics jet lag (Adamovich et al., 2017). In addition, chromatin immunoprecipitation studies revealed HIF1 α occupancy on the promoters of numerous core clock genes such as *PER1*, *PER2*, and *CRY1* (Peek et al., 2017; Wu et al., 2017). Conversely, the core circadian clock modulates HIF1 α . In mouse liver, *Hif1 α* mRNA may be expressed in a circadian manner (Wu et al., 2017), although this has not been observed consistently (Koike et al., 2012; Panda et al., 2002; Ueda et al., 2002). Mouse fibroblasts deficient in CRYs or PERs exhibit elevated levels of HIF1 α protein accumulation upon exposure to hypoxia mimetics, with the opposite phenotype observed in cells lacking BMAL1 (Peek et al., 2017; Wu et al., 2017; Dimova et al., 2019), which has been attributed to BMAL1-driven transcription of *Hif1 α* mRNA. Further suggesting direct cross talk between hypoxia responsive and circadian transcriptional networks, studies utilizing luciferase reporters driven by canonical hypoxia (HRE) and circadian (E-Box) elements have demonstrated that overexpressed BMAL1/HIF1 α heterodimeric complexes can activate both pathways (Peek et al., 2017).

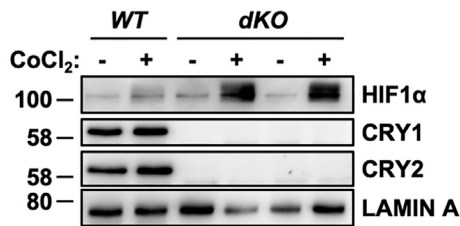
Here, we report that primary myotubes from mice lacking *Cry1* and/or *Cry2* exhibit increased induction of hypoxia target genes in response to limited oxygen or to small molecules that mimic the effects of hypoxia, compared with WT controls. Intriguingly, *Cry2*^{-/-} cells uniquely display enhanced accumulation of HIF1 α protein in the absence of changes in *Hif1 α* mRNA. We find that overexpressed HIF1 α interacts with BMAL1, and this requires several amino acids that are conserved between BMAL1 and ARNT (also known as HIF1 β). Both CRY1 and CRY2 can interact with and repress BMAL1/HIF1 α heterodimers. Furthermore, we report interaction of endogenous BMAL1 and endogenous HIF1 α in primary cultured fibroblasts. Together, these data support a model in which CRY1 and CRY2 suppress HIF1 α -mediated gene expression, through a combination of transcriptional repression by CRY1 and/or CRY2 and post-translational regulation uniquely involving CRY2. Finally, we demonstrate that CRY2-deficient primary myotubes are more glycolytic than WT controls under normoxic conditions and are less responsive to hypoxia. Together, these findings reveal that the circadian repressors CRY1 and CRY2 play an unexpectedly direct role in suppressing hypoxia signaling.

RESULTS

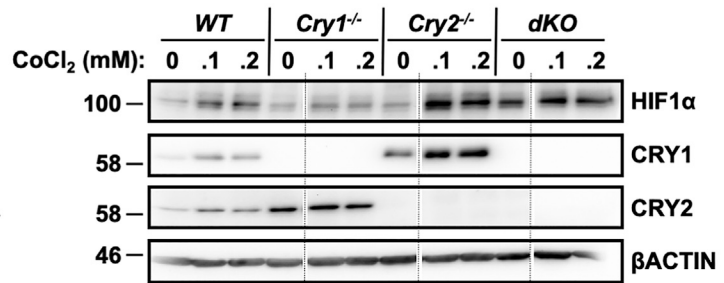
Cryptochromes Suppress HIF1 α Protein Levels and Hypoxia-Induced Transcription

We previously demonstrated that quadriceps muscles from mice lacking both CRY1 and CRY2 exhibit increased activation of hypoxia-regulated genes in response to exercise (Jordan et al., 2017). In addition, the core clock regulates *Hif1 α* transcription (Peek et al., 2017; Wu et al., 2017) and the circadian transcriptional activator BMAL1 is required for the recruitment of HIF1 α to a subset of its target genes in response to hypoxia (Wu et al., 2017). We measured HIF1 α protein in WT and CRY-deficient primary myotubes upon exposure to cobalt chloride (CoCl₂), which inhibits both hydroxylation of HIF1 α and its interaction with the vHL factor (Yuan et al., 2003) and found that its accumulation is greatly enhanced in myotubes lacking both CRY1 and CRY2 (Figure 1A). Both *Cry1*^{-/-};*Cry2*^{-/-} (dKO) and *Cry2*^{-/-} fibroblasts exposed to CoCl₂

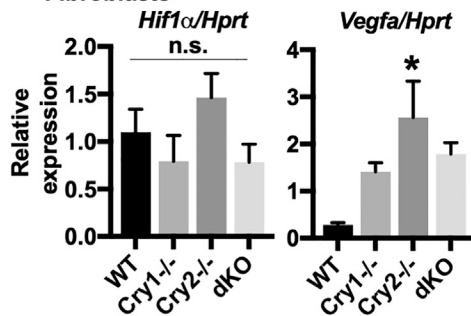
A Myotubes



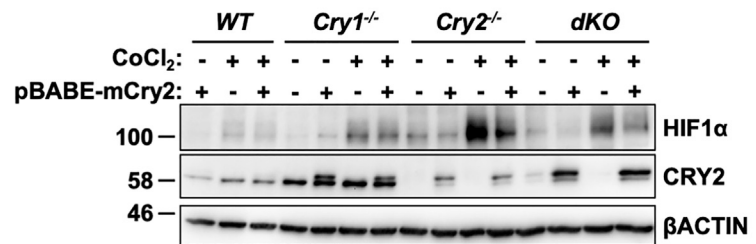
B Fibroblasts



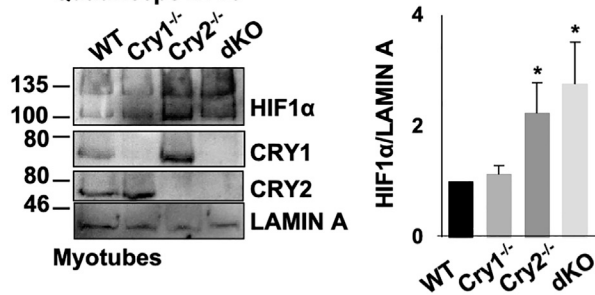
C Fibroblasts



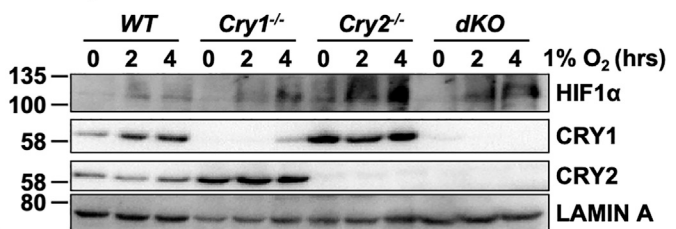
D Fibroblasts



E Quadriceps ZT16



F Myotubes



G

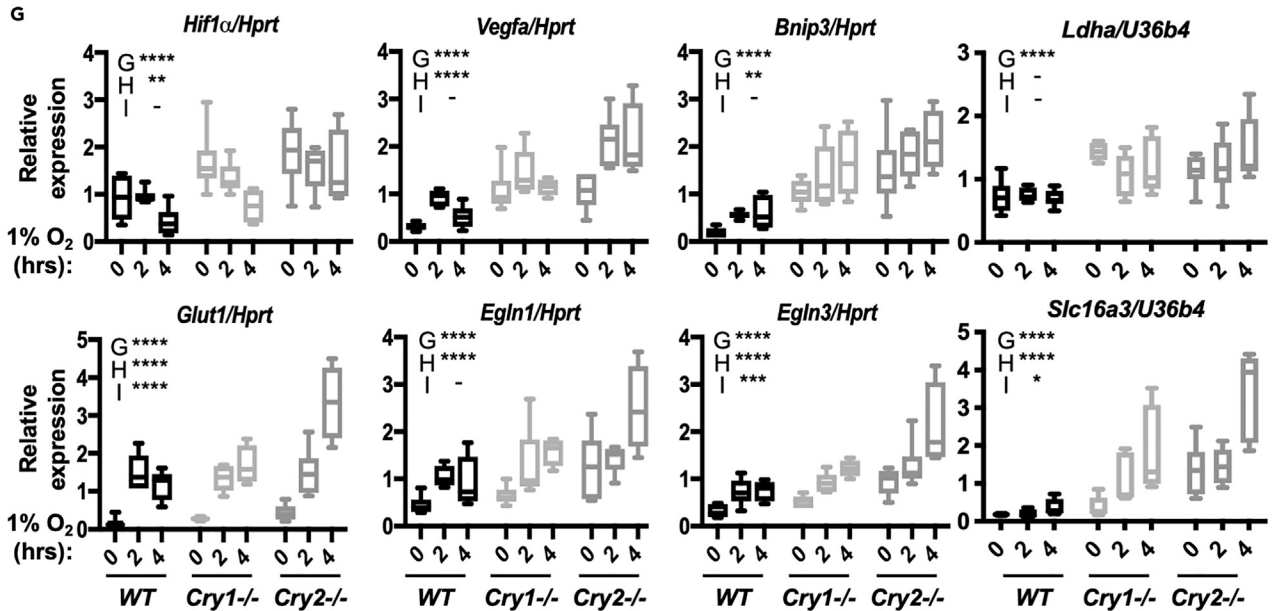


Figure 1. CRYs Suppress HIF1 α

(A) Accumulation of HIF1 α protein detected by immunoblot (IB) in unsynchronized primary myotubes (1 $^{\circ}$ MTs) isolated from *WT* and *dKO* mice and treated with vehicle control or 100 μ M CoCl $_2$. Two technical replicates are shown for *dKO* 1 $^{\circ}$ MTs.
 (B) Accumulation of HIF1 α protein detected by IB in ear fibroblasts (EFs) isolated from *WT*, *Cry1* $^{-/-}$, *Cry2* $^{-/-}$, and *dKO* mice and treated with vehicle control or 0–0.2 mM CoCl $_2$. Faint vertical lines indicate where blot images were spliced to remove samples treated with 50 μ M CoCl $_2$.
 (C) Expression of the indicated transcripts measured by quantitative PCR (qPCR) in fibroblasts of the indicated genotypes, normalized to *Hprt*.
 (D) Accumulation of HIF1 α protein detected by IB in EFs isolated from mice of the indicated genotype and infected with virus carrying either empty vector or pBABE-mCry2 plasmid, before treatment with vehicle control (–) or 100 μ M CoCl $_2$ (+). (Note: the faint CRY2 signal in lane 12 reflects a small amount of sample from lane 13 that spilled into the neighboring well).
 (E) Left, accumulation of HIF1 α protein detected by IB in nuclei of cells isolated from quadriceps muscles of mice of the indicated genotype at ZT16. Right, quantitation of three experiments performed as shown at left.
 (F) Accumulation of HIF1 α protein detected by IB in unsynchronized 1 $^{\circ}$ MTs isolated from mice of the indicated genotype upon exposure to 1% O $_2$ for 0–4 h.
 (G) Expression of the indicated transcripts measured by qPCR in unsynchronized 1 $^{\circ}$ MTs plated under parallel conditions as those in (F). For (C and E), data represent the mean + SD for 3 samples per condition. **p* < 0.05 versus *WT* by one-way ANOVA with Dunn's multiple comparison test. In (G) data represent the range (min to max with mean \pm SD shown in box) for 6 samples per condition, each measured in triplicate. ***p* < 0.01, ****p* < 0.001, *****p* < 0.0001 for a main effect of genotype (G), hypoxia (H), or an interaction between the two, determined by two-way ANOVA. Results of post-hoc analysis are not shown to highlight the main effect results of two-way ANOVA. The position of molecular weight markers (in kDa) are shown to the left of all western blot images. Note that overexpressed epitope-tagged proteins are slightly larger than endogenous ones.
 See also [Figure S1](#).

also express greater levels of HIF1 α protein ([Figures 1B](#), [S1A](#), and [S1B](#)), whereas *Cry1* $^{-/-}$ fibroblasts exhibit lower levels of HIF1 α accumulation in response to CoCl $_2$. Prior reports attributed increased HIF1 α in cells that lack both *Cry1* and 2 ([Peek et al., 2017](#)) or both *Per1* and 2 ([Wu et al., 2017](#)) to enhanced *Hif1 α* transcription due to loss of the repressive arm of the circadian clock ([Dimova et al., 2019](#)). However, we find that whereas loss of *Cry2* phenocopies *dKO* cells in terms of increased HIF1 α protein, loss of the circadian repressor *Cry1* exhibits the opposite phenotype. Furthermore, we did not detect changes in *Hif1 α* mRNA in CRY-deficient fibroblasts ([Figure 1C](#)). We acknowledge that this may be due to the specific cell type examined in this study, as prior reports utilizing mouse embryonic fibroblasts did detect changes in *Hif1 α* mRNA in CRY-deficient cells ([Wu et al., 2017](#); [Dimova et al., 2019](#)). Strikingly, all the *Cry*-deficient fibroblasts exhibited increased induction of the HIF1 α target gene *Vegfa*, even though HIF1 α protein levels were diminished in *Cry1* $^{-/-}$ cells. To determine whether deletion of *Cry2* caused the observed enhanced HIF1 α protein accumulation in *Cry2* $^{-/-}$ and *dKO* cells, we used a retrovirus to ectopically express CRY2 in fibroblasts of various *Cry* background genotypes ([Figure 1D](#)). Indeed, ectopic expression of *Cry2* reduced HIF1 α levels in *Cry2* $^{-/-}$ and *dKO* fibroblasts, but not in cells lacking *Cry1*, demonstrating that the elevation of HIF1 α in *Cry2*-deficient cells is caused by the absence of *Cry2*. Of note, mutants lacking *Cry1* express high basal levels of endogenous *Cry2*, which may explain the lack of observable effect of exogenous overexpression of mCRY2 in these cells. HIF1 α protein is reported to exhibit daily fluctuations in kidney, brain, and quadriceps muscle from sedentary mice or rats, peaking in the early night ([Adamovich et al., 2017](#); [Sato et al., 2019](#)). We measured HIF1 α protein in quadriceps nuclear fractions prepared from *WT*, *Cry1* $^{-/-}$, *Cry2* $^{-/-}$, and *dKO* mice at zeitgeber time (ZT, hours after lights on) 16, when CRY2 protein expression is normally high. As in fibroblasts and myotubes, quadriceps nuclei from mice lacking *Cry2* contain increased HIF1 α ([Figure 1E](#)). Notably, reduced levels of endogenous BMAL1 were detected in quadriceps nuclear extracts from CRY1/2-deficient mice compared with *WT* littermates ([Figure S1C](#)), indicating that increased HIF1 α abundance cannot be attributed to increased BMAL1.

In *WT* primary myotubes, exposure to 1% oxygen increased HIF1 α protein and induced transcription of HIF target genes within 2 h, whereas *Hif1 α* transcript itself was not significantly induced until much later ([Figures S1D](#) and [S1E](#)). Examination of *WT*, *Cry1* $^{-/-}$, *Cry2* $^{-/-}$, and *dKO* myotubes in the same protocol revealed more rapid accumulation of HIF1 α protein in cells lacking *Cry2* ([Figure 1F](#)). In myotubes, *Hif1 α* mRNA was slightly elevated, and hypoxia target gene expression was basally elevated in all cryptochrome mutants, especially in those lacking *Cry2*, and was further induced by hypoxia ([Figure 1G](#)). Although we did not examine HIF2 α specifically in this study, some studies suggest that *Egln3* is primarily regulated by HIF2 α ([Dengler et al., 2014](#)), and we found that this transcript is elevated in CRY-deficient cells. *Ldha* and *Slc16a3* are thought to be primarily regulated by HIF1 α ([Rathmell and Chen, 2008](#)), and their expression is increased in cells lacking cryptochromes. Basal *Hif1 α* expression was unaffected by the absence of CRY1 and/or CRY2 in fibroblasts exposed to CoCl $_2$, but the transcriptional response to hypoxia was accelerated in *Cry2* $^{-/-}$ and *dKO* cells ([Figure S1F](#)). These data indicate that both cryptochromes influence hypoxia target gene transcription, and cells lacking *Cry2* mount an especially rapid transcriptional response, perhaps due to increased HIF1 α protein.

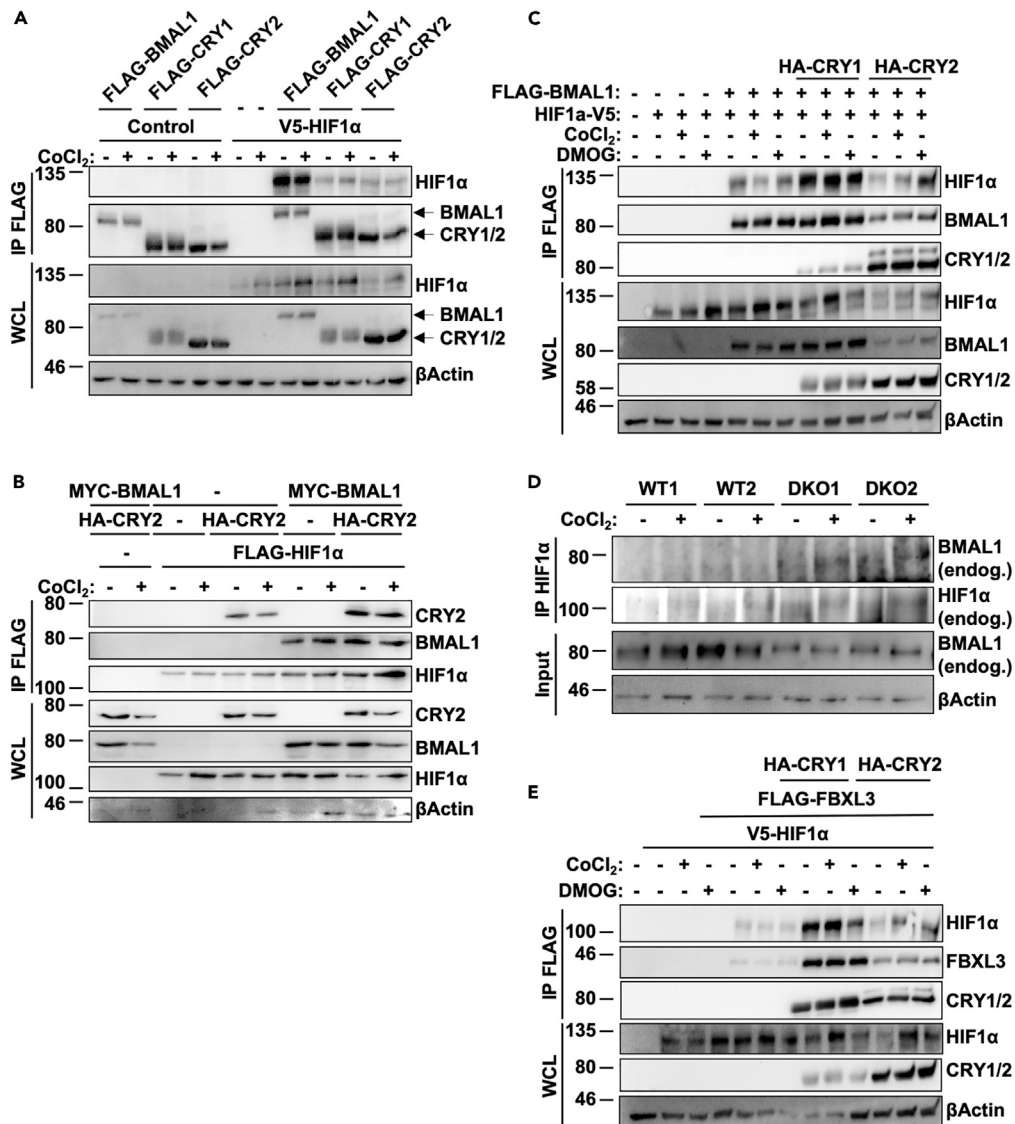


Figure 2. HIF1 α Interacts with the Core Clock Machinery

(A–E) (A–C and E) Proteins detected by immunoblotting (IB) in whole-cell lysates (WCL) or following immunoprecipitation (IP) of the FLAG tag from lysates of HEK293T cells expressing the indicated plasmids and treated with vehicle control (–), 100 μ M CoCl₂, or 200 μ M DMOG as indicated. (D) Endogenous BMAL1, HIF1 α , and β -ACTIN detected in WCL or following IP of HIF1 α from lysates of ear fibroblasts of the indicated genotypes treated with vehicle control (–) or 100 μ M CoCl₂.

Together, these results suggest that both CRY1 and CRY2 can suppress HIF1 α -mediated transcription, whereas CRY2 may have a more dominant role in modulating HIF1 α abundance in the cell types examined.

HIF1 α Interaction with BMAL1 Facilitates Interaction with Circadian Proteins

bHLH-PAS family proteins form heterodimeric complexes consisting of class I and class II subunits. Class I proteins are thought to be highly regulated and expressed in a tissue-specific manner, whereas class II subunit proteins are ubiquitously expressed. The generation of circadian rhythms in mammals is driven by the class I protein CLOCK interacting with its class II partner BMAL1 (Fribourgh and Partch, 2017). Multiple studies have indicated direct interaction between BMAL1 and the class I protein HIF1 α (Hogenesch et al., 1998; Wu et al., 2017), and have implicated BMAL1 in modulation of HIF1 α -driven gene transcription (Wu et al., 2017). Consistent with those prior reports, we found that HIF1 α co-immunoprecipitated with overexpressed BMAL1, CRY1, or CRY2, with a clear preference for interaction with BMAL1 (Figure 2A).

When HIF1 α , BMAL1, and CRYs are co-expressed, the presence of BMAL1 enhances co-immunoprecipitation of CRY2 with HIF1 α (Figure 2B). Notably, overexpression of CRY2 consistently reduces the steady-state levels of HIF1 α protein present in cell lysates (Figures 2A–2C), whereas CRY1 does not appear to alter HIF1 α protein levels as consistently, and enhances the co-immunoprecipitation of HIF1 α with BMAL1 (Figure 2C). Consistent with these observations, we detected endogenous BMAL1 in HIF1 α -containing complexes immunoprecipitated from fibroblast lysates (Figure 2D), suggesting that these proteins interact in mammalian cells. Notably, more BMAL1 was detected in HIF1 α -containing complexes precipitated from CRY-deficient cells despite reduced levels of BMAL1 protein present in the lysates.

We previously demonstrated a role for CRY2 as a co-factor in the SCF^{FBXL3}-mediated degradation of the oncoprotein c-MYC (Huber et al., 2016). To investigate whether a similar mechanism could be involved in CRY2-mediated turnover of HIF1 α , we examined whether HIF1 α and FBXL3 can interact. We found that FBXL3 can bind HIF1 α , and that this interaction is greatly enhanced in the presence of either CRY1 or CRY2. In addition, overexpression of CRY2 reduces both total HIF1 α and FLAG-FBXL3 compared with CRY1 (Figure 2E), suggesting that CRY2 could play a more prominent role in promoting degradation of HIF1 α -containing complexes compared with CRY1. Indeed, whereas HIF1 α is increased in the presence of either BMAL1 alone or simultaneous overexpression of BMAL1/CRY1, the presence of CRY2 decreases both total HIF1 α and BMAL1 (Figure 2C). Together, these results suggest a possible role for a FBXL3/CRY2 complex in directing HIF1 α protein for degradation.

BMAL1-HIF1 α Interaction Involves Their bHLH and PAS Domains

The two main distinguishing features of the bHLH-PAS proteins, the eponymous bHLH and PAS domains, serve distinct functions within these proteins. The bHLH region binds DNA, and the PAS fold is involved in heterodimerization between family members (Kewley et al., 2004). Although all bHLH-PAS proteins exhibit high levels of sequence conservation within their PAS domains, sequence alignments reveal a higher level of conservation among family members regulating the same pathway (Fribourgh and Partch, 2017). In addition, crystal structures of canonical BMAL1/CLOCK and HIF1 α /HIF1 β complexes exhibit distinct spatial arrangements of the PAS domains (Fribourgh and Partch, 2017). Taken together, these results suggest that subtle variations in sequence among various bHLH-PAS members allows for markedly divergent spatial organization of the complexes they form, and thus for highly specific regulation of downstream transcriptional networks. Given our data demonstrating interactions between BMAL1 and HIF1 α , as well as previous reports of transcriptionally active BMAL1/HIF1 α complexes (Peek et al., 2017; Wu et al., 2017), we investigated which region(s) of these proteins were required for heterodimerization.

To define the regions required for interaction between HIF1 α and BMAL1, we generated a series of truncation mutants for each protein and tested their ability to interact in co-immunoprecipitation assays (Figures S2A–S2D). The strongest interactions occur with full-length proteins, whereas a truncated BMAL1 containing the bHLH and PAS-A domains robustly interacts with both CLOCK and HIF1 α (Figures S2A and S2B). Similarly, a truncated version of HIF1 α containing only the bHLH and PAS domains interacts robustly with both BMAL1 and ARNT (Figures S2C and S2D). These data suggest a conserved mode of interaction between various bHLH-PAS proteins, involving primarily the amino-terminal bHLH and PAS domains.

BMAL1 Enhances CRY2 Interaction with HIF1 α

A 2015 study investigating the quaternary structure of various bHLH-PAS heterodimers revealed significant differences in the architecture of HIF2 α -HIF1 β and BMAL1-CLOCK complexes, despite the high level of sequence conservation in the bHLH and PAS domains (Wu et al., 2015). HIF2 α and HIF1 β form an asymmetric structure that involves contacts between the bHLH and PASA/B regions of each protein at six distinct interfaces. Of these six interfaces, mutations introduced at interfaces 1–4 had the greatest impact on heterodimer stability, suggesting that these regions are vital for HIF2 α /HIF1 β interaction. Importantly, mutations affecting the interaction between HIF2 α and HIF1 β also destabilized HIF1 α /HIF1 β heterodimer formation, confirming that these two heterodimers share a similar architecture. Of the six interfaces formed between HIF2 α /HIF1 β , three are conserved in BMAL1/CLOCK heterodimers, suggesting some shared modes of interaction, despite an overall dissimilar three-dimensional architecture. We generated a series of point mutations in BMAL1 analogous to those in HIF1 β (ARNT) that disrupt interaction between HIF1 α /HIF1 β (Figures 3A and 3B). Of the five mutations examined, L115E and V119D consistently decrease interaction between BMAL1 and HIF1 α (Figure 3C). Two mutations located closer to the C terminus (A154D, R343A) did not significantly disrupt interaction between BMAL1 and HIF1 α , but did impair the ability of

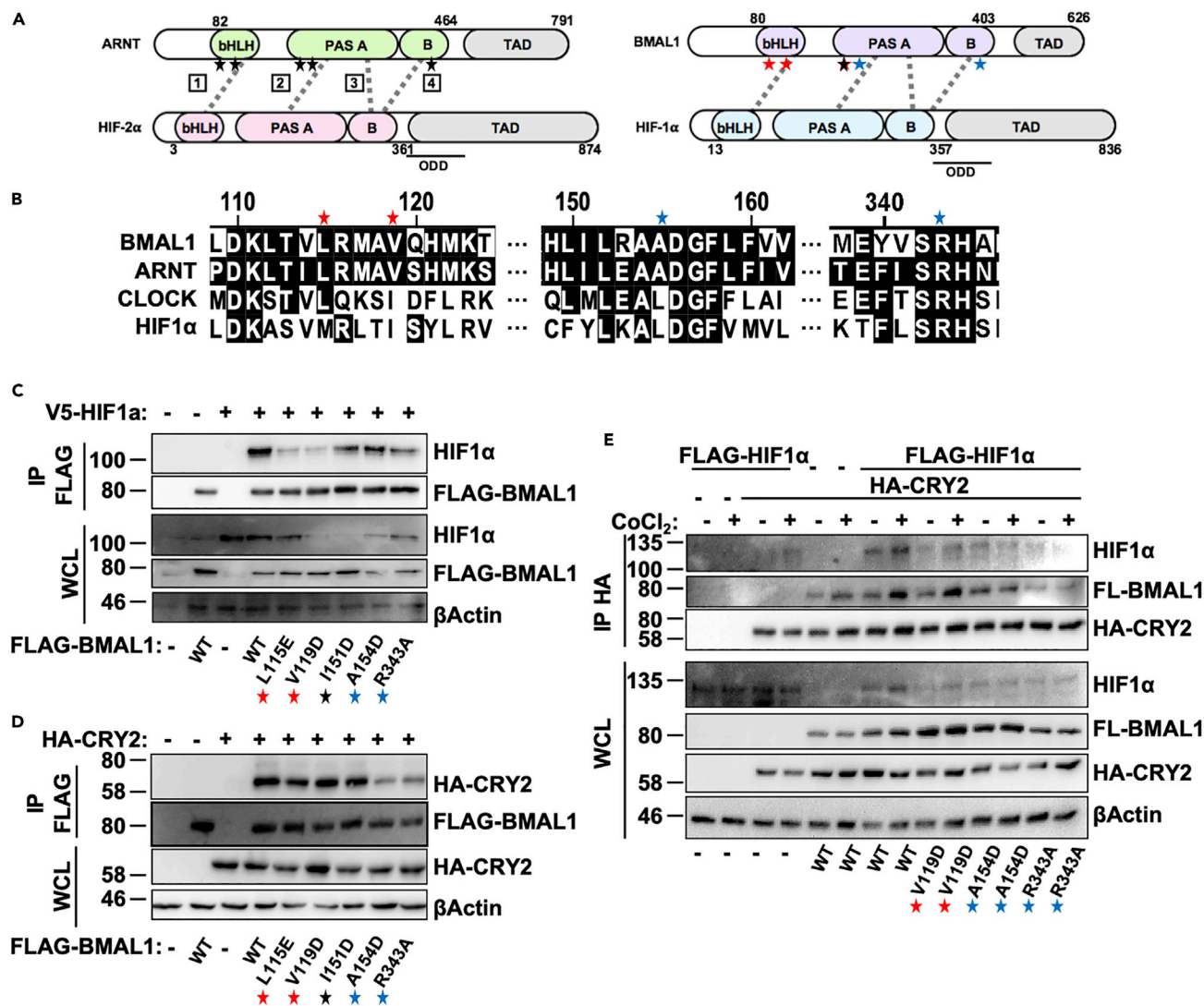


Figure 3. HIF1 α Interacts with Clock Proteins via Unique Domains

(A) Schematic diagram depicting five residues in the ARNT protein described in Wu et al. (2015) as critical for interaction between ARNT and HIF2 α , as well as the location of the corresponding residues in BMAL1 (also known as ARNTL). Gray dashed lines depict interactions between interfaces of each heterodimer pair. Red stars indicate residues found to be critical for interaction between BMAL1 and HIF1 α , whereas blue stars indicate residues found to be critical for BMAL1/CRY2 interaction.

(B) Sequence conservation between bHLH-PAS family proteins in the 115–343 amino acid region where mutations were introduced.

(C–E) Proteins detected by immunoblotting (IB) following immunoprecipitation (IP) of the FLAG (C and D) or hemagglutinin (HA) (E) tags from lysates of HEK293T cells expressing the indicated plasmids and treated with either vehicle control (–) or 100 μ M CoCl₂ (+). See also Figure S2.

BMAL1 to pull down CRY2 (Figure 3D), suggesting that BMAL1 interacts with HIF1 α and CRY2 independently. In contrast, none of the mutants examined impaired the ability of BMAL1 to interact with CRY1 in cells (Figure S2E), indicating that the given point mutations specifically disrupt BMAL1/CRY2 binding, rather than globally disrupting the protein structure of BMAL1, although the altered interaction likely depends on conformational rearrangement. We used point mutations in BMAL1 that independently disrupt interactions with HIF1 α or CRY2 to investigate whether the interaction between HIF1 α and CRY2 involves the formation of a trimeric complex with BMAL1. While full-length BMAL1 increased the ability of CRY2 to pull down HIF1 α , this effect was abrogated by mutations in BMAL1 that decreased either BMAL1/HIF1 α or BMAL1/CRY2 interaction (Figure 3E). These results indicate that maximal interaction between HIF1 α and CRY2 requires BMAL1.

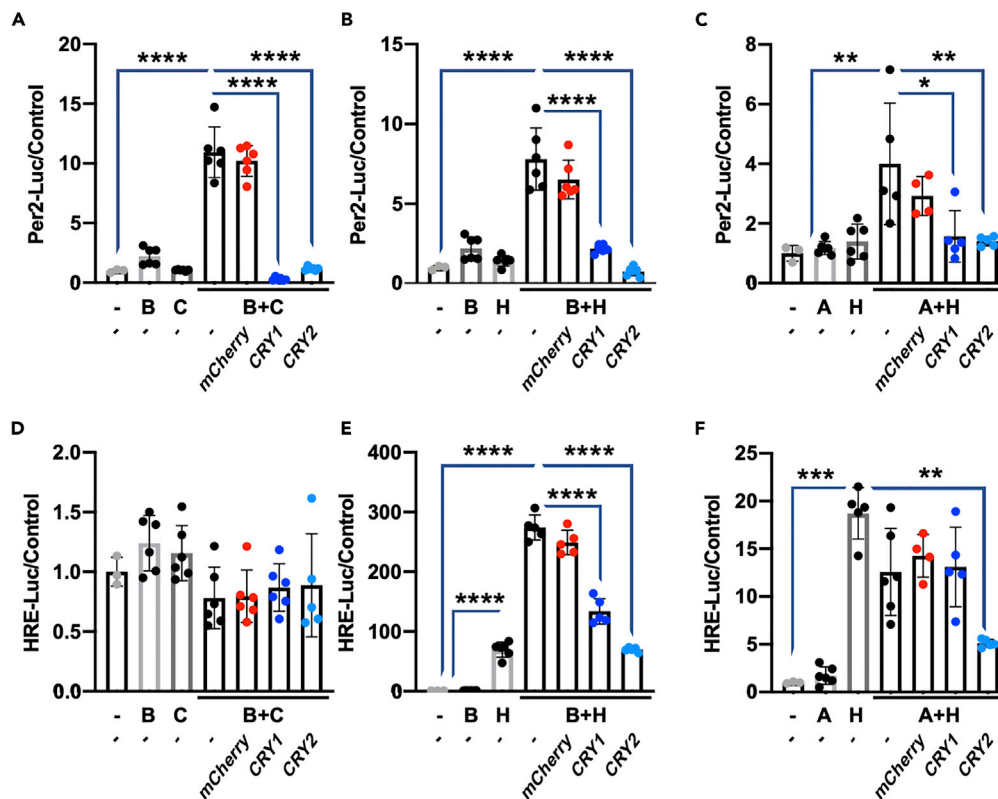


Figure 4. CRYs Repress BMAL1-Containing Heterodimers

(A–F) Luciferase activity in U2OS cells expressing *Per2:Luciferase* (A–C) or *HRE:Luciferase* (D–F). Activation of the reporter is achieved by transfection of the indicated plasmids (B, BMAL1; C, CLOCK; H, HIF1 α). mCherry was used as a negative control, and luminescence was normalized to Renilla luciferase activity. Data represent the mean + SD superimposed with 3–11 individual replicates per condition from a representative of at least three experiments. * $p \leq 0.05$, ** $p \leq 0.01$, *** $p \leq 0.001$, **** $p < 0.0001$ by one-way ANOVA.

Cryptochromes Can Repress Transcriptional Activity of HIF1 α -Containing Heterodimers

Consistent with earlier reports, we find that HIF1 α and BMAL1 can interact. Furthermore, we find that cryptochromes can associate with HIF1 α /BMAL1 heterodimers. HIF1 α /BMAL1 has been reported to recognize both canonical circadian (E-Box) and hypoxia (HRE) promoter elements (Peek et al., 2017), and deletion of BMAL1 prevents recruitment of HIF1 α to a subset of HREs in response to hypoxia (Wu et al., 2017). It is well established that cryptochromes repress BMAL1/CLOCK-driven transcription (Takahashi, 2017), and this can be observed in controlled assays using the E-Box-containing *Per2:Luciferase* reporter (Kriebs et al., 2017). Less is known about the ability of CRYs to influence BMAL1/HIF1 α -driven transcription. Because we found that deletion of cryptochromes influences the transcriptional response to hypoxia, we examined whether cryptochromes can repress HIF1 α -dependent activation of luciferase reporters driven by circadian elements and/or HREs. We found that *Per2-Luciferase* can be induced by either BMAL1/CLOCK or BMAL1/HIF1 α complexes, and that each is repressed by CRYs to a similar extent (Figures 4A and 4B). Importantly, neither BMAL1 nor HIF1 α alone activates *Per2-Luciferase*. Overexpression of ARNT with HIF1 α results in a slight activation of *Per2-Luciferase* that is also suppressed by overexpression of CRYs (Figure 4C). Conversely, *HRE:luciferase* is not activated by BMAL1/CLOCK (Figure 4D). However, it is induced by HIF1 α alone (Figure 4E). BMAL1 does not activate *HRE-Luciferase* alone, but co-expression of BMAL1 with HIF1 α robustly enhances the activation of *HRE-Luciferase* and both CRY1 and CRY2 suppress the additional activation conferred by BMAL1 (Figure 4E). These results suggest that repression of HIF1 α by cryptochromes occurs primarily via BMAL1. Surprisingly, whereas expression of HIF1 α alone activated the *HRE:Luciferase* promoter, simultaneous overexpression of ARNT did not further increase *HRE:Luciferase* in U2OS cells under the conditions used. It is possible that ARNT competes with endogenous BMAL1 for interaction with HIF1 α ; because BMAL1 contains a transcriptional activation domain (TAD) that ARNT does not, dimerization of BMAL1/HIF1 α would be expected to exhibit greater activation of this promoter, and indeed this has also been observed in C2C12 cells (Peek et al., 2017). Overexpression of CRY2 decreases

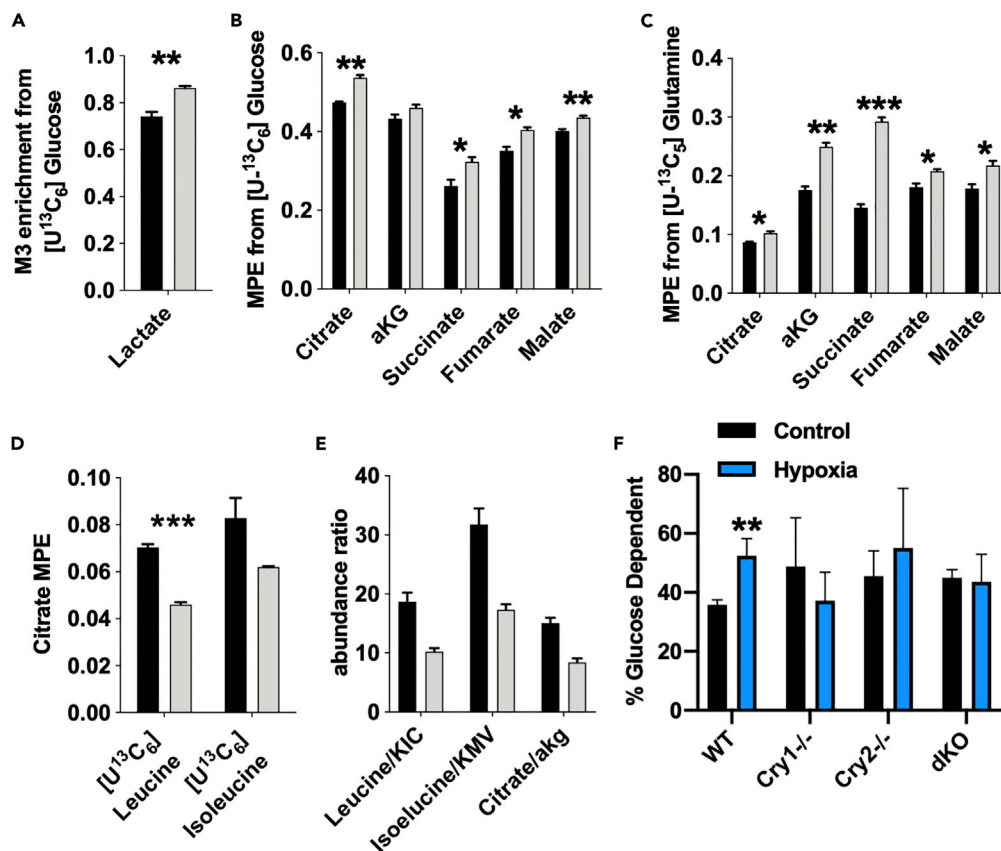


Figure 5. CRYs alter Muscle Metabolic Profile

(A–E) Stable isotope tracing analysis and metabolite abundance performed in primary myotubes (1° MTs) from mice of the indicated genotype. Fractional enrichment (A) or mole percent enrichment (MPE) (B–D) in metabolites following addition of indicated tracer for 24 h. For (A–E), data represent the mean \pm SEM of 3 replicates per condition, which are representative of 3 independent experiments. * $p < 0.05$, ** $p < 0.01$, *** $p < 0.001$ from two-tailed Student's *t* test.

(F) Glucose dependency measured in unsynchronized 1° MTs isolated from mice of the indicated genotype and treated with either vehicle control (black) or 100 μ M CoCl_2 (blue). ** $p \leq 0.01$ versus control by *t* test using two-stage linear step-up procedure of Benjamini, Krieger, and Yekutieli, with $Q = 5\%$. Data in (F) represent the mean \pm SEM of the results from 4 independent experiments.

See also [Figure S3](#).

ARNT + HIF1 α -dependent HRE-Luciferase expression ([Figure 4F](#)), possibly by impacting HIF1 α protein abundance. Furthermore, others have shown that the bHLH-PAS family of transcription factors exhibit promiscuous dimerization patterns with proteins other than their canonical binding partners ([Wu et al., 2016](#)). Further investigation will be required to fully understand the role of cryptochromes in repressing the activity of these complexes.

Deletion of Cryptochromes Enhances Glycolysis in Myotubes

Metabolic tracing analysis conducted in *WT* and *dKO* myotubes revealed that cells lacking cryptochromes exhibited increased enrichment in lactate and Krebs cycle intermediates from [U- $^{13}\text{C}_6$]glucose ([Figures 5A](#) and [5B](#)); *dKO* cells also had higher enrichment in Krebs cycle intermediates from [U- $^{13}\text{C}_5$]glutamine compared with *WT* cells ([Figure 5C](#)). In contrast, *dKO* cells exhibit reduced catabolism of the branched-chain amino acids (BCAAs) leucine and isoleucine ([Figure 5D](#)). Consistent with these trends, we observed a significant decrease in the ratio of the abundance of BCAAs to their respective branched keto acids and citrate/ α KG ([Figure 5E](#)), suggesting decreased branched-chain keto acid dehydrogenase (BCKDH) activity and increased reductive carboxylation.

Studies utilizing PEO1 ovarian cancer cells demonstrated that depletion of HIF1 α decreases glucose dependency in a mitochondrial substrate flux assay and overexpression of HIF1 α increases glucose usage

(Kitajima et al., 2017). We used a similar strategy to measure glucose dependency in myotubes to determine whether *Cry1/2* deletion impacts cellular metabolism in a manner consistent with elevated endogenous HIF1 α activity. As expected, WT myotubes exhibited increased glucose dependency upon treatment with the hypoxia mimetic CoCl₂ (Figure 5F). In contrast, *Cry1*^{-/-}, *Cry2*^{-/-}, and *dKO* myotubes tend to have increased basal reliance on glucose, with hypoxia treatment failing to increase glucose dependency. No significant differences in glutamine or fatty acid dependency were observed for any of the conditions examined (Figures S3A and S3B). These metabolic analyses in *Cry1/2*-deficient myotubes suggest that the loss of cryptochromes alters skeletal muscle metabolism in a manner consistent with enhanced HIF1 α activity. Furthermore, our findings support prior studies suggesting that hypoxia and HIF1 α strongly influence Krebs cycle and amino acid metabolism. Consistent with these trends, the most significantly altered metabolites observed in a targeted analysis of homogenized quadriceps muscles of *dKO* compared with WT mice were glutamine and serine (Figure S3C).

DISCUSSION

Studies in rats have indicated not only that levels of oxygen in the blood fluctuate in a circadian manner but also that the relative oxygenation of tissues such as the kidneys exhibits cyclic fluctuations with peak levels during the active phase. Moreover, rhythms in oxygen concentration can synchronize the circadian clocks of cultured cells in a HIF1 α -dependent manner (Adamovich et al., 2017). These results indicate that daily fluctuations in oxygen consumption and behavior, likely driven by the master pacemaker in the suprachiasmatic nucleus, can contribute to indirectly resetting peripheral tissue clocks via HIF1 α . Moreover, HIF1 α protein levels (but not *Hif1 α* mRNA) exhibit daily rhythms in metabolically active tissues such as the kidney and brain (Adamovich et al., 2017). This is important, as it indicates that HIF1 α not only influences the timing of peripheral clocks but also is reciprocally regulated at the level of protein accumulation by circadian clocks. Indeed, reports have indicated that maximal transcriptional activation of hypoxia pathways is gated by circadian timing (Peek et al., 2017; Wu et al., 2017). Together, these results suggest a system in which circadian/hypoxia pathway cross talk allows peripheral tissues to both anticipate repetitive behaviors such as feeding and locomotor activity, as well as to adapt to metabolic challenges such that fuel utilization is coordinated with substrate availability (Schroder and Esser, 2013). This is particularly important in the context of skeletal muscle, which has evolved to maximize metabolic flexibility to adapt to daily fluctuations in fuel source, availability, and demand (Dyar et al., 2014). Indeed, our finding of enhanced basal reliance on glucose in cells lacking the circadian repressors CRY1 and CRY2 combined with the decreased glucose reliance in BMAL1-deficient cells (Dyar et al., 2014) indicates that muscle clocks modulate substrate selection across the day-night cycle.

Training-induced increases in transcriptional networks that mediate a switch between oxidative and glycolytic metabolism contribute to enhanced exercise capacity (Hoppeler et al., 2003). During strenuous exercise, skeletal muscle regularly experiences dramatic fluctuations in the partial pressure of oxygen from 30 mmHg to less than 5 mmHg (Ortiz-Prado et al., 2019), and HIF1 α is critical for the maintenance of ATP production in muscle (Seagroves et al., 2001). Among the mechanisms by which HIF1 α impinges on cellular metabolism are induction of glucose transporters and glycolytic enzymes, induction of PDK1 to actively inhibit PDH conversion of pyruvate to acetyl-CoA, and induction of LDHA for utilization of pyruvate in glycolysis/lactate production (Kim et al., 2006). Thus, conversion from an oxidative to glycolytic phenotype by HIF1 α is not merely a passive response to limiting oxygen supply, but an active shunting of resources away from mitochondrial utilization. Despite intense study of HIF1 α -mediated glycolytic induction in the context of cancer, numerous studies have indicated that HIF1 α functions in a normal physiological context to actively regulate glucose utilization within a fine range of oxygen concentrations. For instance, cells repress tricarboxylic acid (TCA) cycle components and induce glycolytic enzymes under conditions of 2% oxygen, which is not limiting for cellular respiration (Semenza, 2017). Furthermore, it has been demonstrated that HIF1 α -null mouse embryonic fibroblasts (MEFs) actually produce more ATP at 1% O₂ compared with WT cells, but ultimately undergo apoptosis due to excessive ROS production (Kim et al., 2006). Thus, rather than merely being a glycolytic “on/off” switch, HIF1 α functions as a fulcrum with which to balance glucose flux through glycolysis or mitochondrial respiration to limit excessive ROS accumulation under conditions of either hyperoxia or hypoxia (Terraneo et al., 2014).

HIF1 α thus influences exercise capacity via several overlapping pathways: by influencing levels of the glycolytic product and substrate for energy production, lactate (Myers and Ashley, 1997); by maintaining ATP production under low oxygen tension; and by facilitating long-term adaptation to exercise via activation

of downstream genes such as *VEGFA* (Peek et al., 2017). Mice with muscle-specific deletion of HIF1 α fail to induce glycolysis during exercise, and the compensatory increase in muscle oxidative phosphorylation leads to increased tissue damage (Mason et al., 2004). We have previously reported increased exercise capacity in mice lacking both CRY1/2. Although this is undoubtedly influenced by *dKO* mice having increased activation of exercise-adaptive pathways via PPAR δ , *dKO* mice also exhibited elevated activation of hypoxia networks (Jordan et al., 2017). This, along with numerous publications demonstrating induction of HIF1 α transcriptional targets in cells and tissues lacking the repressive arm of the circadian clock make it clear that these two pathways are vital for proper muscle function (Adamovich et al., 2017; Peek et al., 2017; Wu et al., 2017). Intriguingly, comprehensive transcriptional profiling of rodent skeletal muscles revealed striking high expression of *Cry2* in the flexor digitorum brevis (FDB) muscle (Terry et al., 2018). As FDB is composed primarily of glycolytic type IIa/type IIx muscle fibers (Tarpey et al., 2018), this suggests that CRY2 could regulate hypoxic induction in fast-twitch fibers, thus influencing exercise capacity.

We found that cells lacking CRY2 have greatly increased accumulation of HIF1 α protein both under conditions of artificial induction via the hypoxia mimetic CoCl₂ and following prolonged hypoxic exposure. Other studies have noted that a lack of both CRY1 and CRY2 enhances HIF1 α protein levels in both cells and tissues of mice (Adamovich et al., 2017; Peek et al., 2017; Wu et al., 2017; Dimova et al., 2019), whereas here we report individual and opposite effects of the individual cryptochromes on HIF1 α steady-state protein levels. Increased HIF1 α in *dKO* tissues does not appear, therefore, to arise due to a lack of the negative arm of the circadian clock increasing *Hif1 α* transcription, but rather via CRY2-dependent regulation of HIF1 α protein turnover. We find that whereas both CRY1 and CRY2 are capable of repressing transcription of HIF1 α targets, transcription of *Hif1 α* itself is largely unaffected by CRYs. In addition, induction of hypoxia target genes occurs on a far more rapid timescale than does induction of HIF1 α itself in *WT* cells, which supports the finding that HIF1 α is primarily regulated at the protein, rather than transcript, level (Bardos and Ashcroft, 2005). A recent study suggests that CRY1 decreases both HIF1 α half-life and binding to its target gene promoters (Dimova et al., 2019). In our hands, CRY1 appeared to regulate basal transcription of hypoxia target genes, and to repress some HIF1 α -containing heterodimeric complexes from activating an HRE promoter, but had limited impact on HIF1 α protein accumulation. Different roles of CRY1 and CRY2 in modulating HIF1 α protein levels in different cell types could contribute to the divergent observations that we make in muscles and primary muscle cell culture compared with the observations by Dimova and colleagues using fibroblasts. It is likely that regulation of the hypoxic gene network by CRYs occurs at multiple levels, with distinct HIF1 α -containing complexes exhibiting unique regulation by CRY1 and/or CRY2 and other context-dependent factors.

Despite their high level of sequence conservation, CRY1 and CRY2 have divergent roles in repression of the core circadian clock, with single-knockout mutants displaying opposite phenotypes in terms of period length (Vitaterna et al., 1999). CRY1 interacts more strongly with the CLOCK-BMAL1 heterodimer than does CRY2 (Rosensweig et al., 2018) and is believed to be the more critical circadian repressor (Khan et al., 2012). CRY2 is a more efficient repressor of non-clock transcription factors that are targeted by cryptochromes, including nuclear hormone receptors (Kriebs et al., 2017) and c-MYC (Huber et al., 2016). We find that CRY2 also seems to be a stronger regulator of HIF1 α than is CRY1, at least in muscles.

Using two complementary approaches, we found that cells lacking CRYs are more reliant on glucose, consistent with the concept that both CRY1 and CRY2 repress HIF1 α -dependent transcriptional networks. This is in line with prior reports that loss of BMAL1 in skeletal muscle decreases glucose reliance and suggests that modulation of either the negative or the positive arms of the clock influence substrate preference (Harfmann et al., 2016). We also observed increased glutamine enrichment in TCA intermediates in *dKO* cells, consistent with a hypoxic metabolic phenotype (Vacanti et al., 2014). Although we did not find increased "glutamine dependency" when assessing oxygen consumption in the presence of the glutaminase inhibitor BPTES, this apparent discrepancy may be due to the cells' ability to compensate when the glutamine pathway is inhibited, as glutamine contributes significantly less to TCA cycle activity in primary myotubes compared with other cell types such as cancer cells (Vacanti et al., 2014). Although we found that *dKO* cells exhibit reduced incorporation of labeled BCAAs into citrate, they do not accumulate excess BCAAs but rather contain low levels of leucine and isoleucine relative to their respective ketoacids, KIC and KMV. This suggests that in *dKO* cells branched-chain amino acid transaminase (BCAT), which is responsible for conversion of BCAAs to ketoacids, is active but that *dKO* cells lack some downstream activity in

this pathway, such as the BCKDH complex. Consistent with this model, some of us recently demonstrated that BCKDH activity is reduced under conditions of hypoxia (Wallace et al., 2018). Increased glucose flux in *dKO* cells combined with an inability to utilize BCAAs highlights the functional impact of CRY-mediated regulation of HIF1 α .

Circadian regulation of the hypoxic response seems to reflect a complex interplay of transcriptional and post-translational regulation by CRYs. HIF1 α protein turnover is driven by several pathways, the best characterized of which involves oxygen-dependent interaction with the vHL ubiquitin ligase (Ivan and Kaelin, 2017). HIF1 α is also subject to autophagic degradation by both vHL-dependent and vHL-independent mechanisms (DePavia et al., 2016). Recently, it was demonstrated that CRYs are also susceptible to degradation via macroautophagy (Toledo et al., 2018). Further investigation will be required to understand how CRY2 impacts HIF1 α protein levels.

It has long been suspected that hypoxia and circadian networks interact (Hogenesch et al., 1998). Several reports indicate that BMAL1 can interact with HIF1 α (Bersten et al., 2013; Hogenesch et al., 1998). We and others have shown that HIF1 α can form transcriptionally active complexes with BMAL1 (Egg et al., 2013; Peek et al., 2017; Wu et al., 2017). However, the ability of circadian proteins and HIF1 α to form functional heterodimers in a physiological context has been controversial (Cowden and Simon, 2002). Although HIF1 α /BMAL1 heterodimers are unable to support normal vascularization in HIF1 β -deficient mouse embryos (Cowden and Simon, 2002), it was recently demonstrated that muscle-specific deletion of HIF1 β has no impact whatsoever on muscle vascularization (Badin et al., 2016). This finding suggests that an alternate partner, perhaps BMAL1, may cooperate with HIF1 α to support muscle vascular remodeling. We found that the BMAL1-HIF1 α complex directs transcription of a subset of circadian and hypoxia genes, rather than being functionally redundant to HIF1 α /HIF1 β . The roles of BMAL1 and/or CRYs in regulation of HIF1 α -dependent physiology *in vivo* and how they are integrated with canonical ARNT/HIF1 β signaling remain to be determined.

Although HIF1 α has been most extensively studied in the context of aberrant cell metabolism and cancer progression, it is clearly indispensable for normal physiology. Indeed, knockout of HIF1 α is associated with decreased exercise performance after training (Mason et al., 2004), perhaps due to a loss of regenerative capacity in response to tissue damage (Scheerer et al., 2013). A loss of HIF1 α signaling can induce metabolic crisis due to ATP depletion, whereas overactivation of hypoxic pathways is detrimental for multiple metabolically active tissues (Asai et al., 2017; Mesarwi et al., 2016). Notably, a *Per1/2 dKO* model, which exhibits far greater induction of both *Hif1 α* and target gene transcription than *Cry1/2 dKO* mice, was more susceptible to ischemic cell death in myocardial infarction (Wu et al., 2017).

In a broader physiological context, integration of circadian timing cues with hypoxic gene network activation may serve as a means for skeletal muscle to balance the expected substrate availability arising from predictable feeding/fasting cycles with the immediate need of this tissue to produce energy. Recently, several studies have addressed the impact of time of day on exercise, with HIF1 α networks implicated as one of the major pathways gated by the clock (Ezagouri et al., 2019; Sato et al., 2019). That HIF1 α has itself been demonstrated to alter circadian clock timing in peripheral tissues is intriguing (Adamovich et al., 2017), as it suggests a system through which exercise might increase the robustness of circadian clocks and thus, overall metabolic health. Future research will elucidate the role of circadian/hypoxia cross talk in the context of other oxygen-dependent physiology and pathology.

Limitations of the Study

Although we demonstrate that CRY2 suppresses the accumulation of HIF1 α protein, we have not determined whether this involves modifying HIF1 α stability, or defined the molecular mechanism by which this occurs. Furthermore, although our experiments indicate a more robust regulation of HIF1 α accumulation by CRY2 than by CRY1, we cannot exclude the possibility that this is dependent on cell type or context, especially as others have demonstrated that CRY1 can suppress HIF1 α accumulation (Dimova et al., 2019). Regarding the role of BMAL1 in promoting interaction between cryptochromes and HIF1 α , we cannot conclude that BMAL1 is required for this interaction without examining whether deletion of BMAL1 abolishes the interactions of CRY1/2 with HIF1 α . Finally, although we expect that CRY1 and CRY2 likely suppress HIF2 α , as shown by others (Dimova et al., 2019), we did not study HIF2 α here.

Resource Availability

Lead Contact

Further information and requests for resources and reagents should be directed to and will be fulfilled by the Lead Contact, Katja Lamia (klamia@scripps.edu).

Materials Availability

All unique/stable reagents generated in this study are available from the Lead Contact with a completed Materials Transfer Agreement.

Data and Code Availability

This study did not generate datasets or code.

METHODS

All methods can be found in the accompanying [Transparent Methods supplemental file](#).

SUPPLEMENTAL INFORMATION

Supplemental Information can be found online at <https://doi.org/10.1016/j.isci.2020.101338>.

ACKNOWLEDGMENTS

This work was funded by NIH grants R01 DK097164 (to K.A.L.) and DK112927 (to K.A.L. and C.M.M.); R01CA234245 (to C. M.M.); 1S10OD16357, which funded the Seahorse Instrument at The Scripps Research Institute; and a Searle Scholars award to K.A.L. from the Kinship Foundation. We thank Enrique Saez, Luke Wiseman, Dennis Wolan, Drew Duglan, Marie Pariollaud, and Anne-Laure Huber for helpful discussions; sharing of technical expertise, equipment, and reagents; and/or critical reading of the manuscript, and T. Thomas for administrative assistance.

AUTHOR CONTRIBUTIONS

Conceptualization, M.E.V. and K.A.L., Methodology, M.E.V., M.W., and M.K.H., Validation, M.E.V., M.W., M.K.H., K.A.L., and C.M.M., Formal Analysis, M.E.V., M.W., M.K.H., C.M.M., and K.A.L., Investigation, M.E.V., M.W., M.K.H., and A.B.C., Writing – Original Draft, M.E.V., Writing – Review and Editing, M.E.V., M.W., M.K.H., A.B.C., C.M.M., and K.A.L., Visualization, M.V., M.W., M.K.H., and K.A.L., Supervision, C.M.M. and K.A.L., Funding Acquisition, C.M.M. and K.A.L.

DECLARATION OF INTERESTS

Authors declare no conflict of interest.

Received: March 4, 2020

Revised: May 13, 2020

Accepted: July 1, 2020

Published: July 24, 2020

REFERENCES

- Adamovich, Y., Ladeuix, B., Golik, M., Koeners, M.P., and Asher, G. (2017). Rhythmic oxygen levels reset circadian clocks through HIF1alpha. *Cell Metab.* 25, 93–101.
- Asai, Y., Yamada, T., Tsukita, S., Takahashi, K., Maekawa, M., Honma, M., Ikeda, M., Murakami, K., Munakata, Y., Shirai, Y., et al. (2017). Activation of the hypoxia inducible factor 1alpha subunit pathway in steatotic liver contributes to formation of cholesterol gallstones. *Gastroenterology* 152, 1521–1535.e8.
- Badin, P.M., Sopariwala, D.H., Lorca, S., and Narkar, V.A. (2016). Muscle Arnt/Hif1beta is dispensable in myofiber type determination, vascularization and insulin sensitivity. *PLoS One* 11, e0168457.
- Bardos, J.I., and Ashcroft, M. (2005). Negative and positive regulation of HIF-1: a complex network. *Biochim. Biophys. Acta* 1755, 107–120.
- Bersten, D.C., Sullivan, A.E., Peet, D.J., and Whitelaw, M.L. (2013). bHLH-PAS proteins in cancer. *Nat. Rev. Cancer* 13, 827–841.
- Cowden, K.D., and Simon, M.C. (2002). The bHLH/PAS factor MOP3 does not participate in hypoxia responses. *Biochem. Biophys. Res. Commun.* 290, 1228–1236.
- Dengler, V.L., Galbraith, M., and Espinosa, J.M. (2014). Transcriptional regulation by hypoxia inducible factors. *Crit. Rev. Biochem. Mol. Biol.* 49, 1–15.
- DePavia, A., Jonasch, E., and Liu, X.D. (2016). Autophagy degrades hypoxia inducible factors. *Mol. Cell. Oncol.* 3, e1104428.
- Dimova, E.Y., Jakupovic, M., Kubaichuk, K., Mennerich, D., Chi, T.F., Tamanini, F., Oklejewicz, M., Hanig, J., Byts, N., Makela, K.A., et al. (2019). The circadian clock protein CRY1 is a negative regulator of HIF-1alpha. *iScience* 13, 284–304.

- Dyar, K.A., Ciciliot, S., Wright, L.E., Bienso, R.S., Tagliazucchi, G.M., Patel, V.R., Forcato, M., Paz, M.I., Gudiksen, A., Solagna, F., et al. (2014). Muscle insulin sensitivity and glucose metabolism are controlled by the intrinsic muscle clock. *Mol. Metab.* 3, 29–41.
- Egg, M., Koblit, L., Hirayama, J., Schwerte, T., Folterbauer, C., Kurz, A., Fiechtner, B., Most, M., Salvenmoser, W., Sassone-Corsi, P., et al. (2013). Linking oxygen to time: the bidirectional interaction between the hypoxic signaling pathway and the circadian clock. *Chronobiol. Int.* 30, 510–529.
- Ezagouri, S., Zwighaft, Z., Sobel, J., Baillieu, S., Doutreleau, S., Ladeuix, B., Golik, M., Verges, S., and Asher, G. (2019). Physiological and molecular dissection of daily variance in exercise capacity. *Cell Metab.* 30, 78–91.e4.
- Fribourgh, J.L., and Partch, C.L. (2017). Assembly and function of bHLH-PAS complexes. *Proc. Natl. Acad. Sci. U S A* 114, 5330–5332.
- Harfmann, B.D., Schroder, E.A., Kachman, M.T., Hodge, B.A., Zhang, X., and Esser, K.A. (2016). Muscle-specific loss of Bmal1 leads to disrupted tissue glucose metabolism and systemic glucose homeostasis. *Skeletal Muscle* 6, 12.
- Hogenesch, J.B., Gu, Y.Z., Jain, S., and Bradfield, C.A. (1998). The basic-helix-loop-helix-PAS orphan MOP3 forms transcriptionally active complexes with circadian and hypoxia factors. *Proc. Natl. Acad. Sci. U S A* 95, 5474–5479.
- Hoppeler, H., and Vogt, M. (2001). Muscle tissue adaptations to hypoxia. *J. Exp. Biol.* 204, 3133–3139.
- Hoppeler, H., Vogt, M., Weibel, E.R., and Fluck, M. (2003). Response of skeletal muscle mitochondria to hypoxia. *Exp. Physiol.* 88, 109–119.
- Huber, A.L., Papp, S.J., Chan, A.B., Henriksson, E., Jordan, S.D., Krieps, A., Nguyen, M., Wallace, M., Li, Z., Metallo, C.M., et al. (2016). CRY2 and FBXL3 cooperatively degrade c-MYC. *Mol. Cell* 64, 774–789.
- Ivan, M., and Kaelin, W.G., Jr. (2017). The EGLN-HIF O₂-sensing system: multiple inputs and feedbacks. *Mol. Cell* 66, 772–779.
- Jordan, S.D., Krieps, A., Vaughan, M., Duglan, D., Fan, W., Henriksson, E., Huber, A.L., Papp, S.J., Nguyen, M., Afetian, M., et al. (2017). CRY1/2 selectively repress PPARdelta and limit exercise capacity. *Cell Metab.* 26, 243–255.e6.
- Kewley, R.J., Whitelaw, M.L., and Chapman-Smith, A. (2004). The mammalian basic helix-loop-helix/PAS family of transcriptional regulators. *Int. J. Biochem. Cell Biol.* 36, 189–204.
- Khan, S.K., Xu, H., Ukai-Tadenuma, M., Burton, B., Wang, Y., Ueda, H.R., and Liu, A.C. (2012). Identification of a novel cryptochrome differentiating domain required for feedback repression in circadian clock function. *J. Biol. Chem.* 287, 25917–25926.
- Kim, J.W., Tchernyshyov, I., Semenza, G.L., and Dang, C.V. (2006). HIF-1-mediated expression of pyruvate dehydrogenase kinase: a metabolic switch required for cellular adaptation to hypoxia. *Cell Metab.* 3, 177–185.
- Kitajima, S., Lee, K.L., Hikasa, H., Sun, W., Huang, R.Y., Yang, H., Matsunaga, S., Yamaguchi, T., Araki, M., Kato, H., et al. (2017). Hypoxia-inducible factor-1alpha promotes cell survival during ammonia stress response in ovarian cancer stem-like cells. *Oncotarget* 8, 114481–114494.
- Koike, N., Yoo, S.H., Huang, H.C., Kumar, V., Lee, C., Kim, T.K., and Takahashi, J.S. (2012). Transcriptional architecture and chromatin landscape of the core circadian clock in mammals. *Science* 338, 349–354.
- Kriebs, A., Jordan, S.D., Soto, E., Henriksson, E., Sandate, C.R., Vaughan, M.E., Chan, A.B., Duglan, D., Papp, S.J., Huber, A.L., et al. (2017). Circadian repressors CRY1 and CRY2 broadly interact with nuclear receptors and modulate transcriptional activity. *Proc. Natl. Acad. Sci. U S A* 114, 8776–8781.
- Liberti, M.V., and Locasale, J.W. (2016). The Warburg effect: how does it benefit cancer cells? *Trends Biochem. Sci.* 41, 211–218.
- Lindholm, M.E., and Rundqvist, H. (2016). Skeletal muscle hypoxia-inducible factor-1 and exercise. *Exp. Physiol.* 101, 28–32.
- Mason, S.D., Howlett, R.A., Kim, M.J., Olfert, I.M., Hogan, M.C., McNulty, W., Hickey, R.P., Wagner, P.D., Kahn, C.R., Giordano, F.J., et al. (2004). Loss of skeletal muscle HIF-1alpha results in altered exercise endurance. *PLoS Biol.* 2, e288.
- Mesarwi, O.A., Shin, M.K., Bevans-Fonti, S., Schlesinger, C., Shaw, J., and Polotsky, V.Y. (2016). Hepatocyte hypoxia inducible factor-1 mediates the development of liver fibrosis in a mouse model of nonalcoholic fatty liver disease. *PLoS One* 11, e0168572.
- Myers, J., and Ashley, E. (1997). Dangerous curves. A perspective on exercise, lactate, and the anaerobic threshold. *Chest* 111, 787–795.
- Ortiz-Prado, E., Dunn, J.F., Vasconez, J., Castillo, D., and Viscor, G. (2019). Partial pressure of oxygen in the human body: a general review. *Am. J. Blood Res.* 9, 1–14.
- Panda, S., Antoch, M.P., Miller, B.H., Su, A.I., Schook, A.B., Straume, M., Schultz, P.G., Kay, S.A., Takahashi, J.S., and Hogenesch, J.B. (2002). Coordinated transcription of key pathways in the mouse by the circadian clock. *Cell* 109, 307–320.
- Peek, C.B., Levine, D.C., Cedernaes, J., Taguchi, A., Kobayashi, Y., Tsai, S.J., Bonar, N.A., McNulty, M.R., Ramsey, K.M., and Bass, J. (2017). Circadian clock interaction with HIF1alpha mediates oxygenic metabolism and anaerobic glycolysis in skeletal muscle. *Cell Metab.* 25, 86–92.
- Rathmell, W.K., and Chen, S. (2008). VHL inactivation in renal cell carcinoma: implications for diagnosis, prognosis and treatment. *Expert Rev. Anticancer Ther.* 8, 63–73.
- Rosensweig, C., Reynolds, K.A., Gao, P., Lathamas, I., Shan, Y., Ranganathan, R., Takahashi, J.S., and Green, C.B. (2018). An evolutionary hotspot defines functional differences between CRYPTOCHROMES. *Nat. Commun.* 9, 1138.
- Sato, S., Basse, A.L., Schonke, M., Chen, S., Samad, M., Altintas, A., Laker, R.C., Dalbram, E., Barres, R., Baldi, P., et al. (2019). Time of exercise specifies the impact on muscle metabolic pathways and systemic energy homeostasis. *Cell Metab.* 30, 92–110.e114.
- Scheerer, N., Dehne, N., Stockmann, C., Swoboda, S., Baba, H.A., Neugebauer, A., Johnson, R.S., and Fandrey, J. (2013). Myeloid hypoxia-inducible factor-1alpha is essential for skeletal muscle regeneration in mice. *J. Immunol.* 191, 407–414.
- Schroder, E.A., and Esser, K.A. (2013). Circadian rhythms, skeletal muscle molecular clocks, and exercise. *Exerc. Sport Sci. Rev.* 41, 224–229.
- Seagroves, T.N., Ryan, H.E., Lu, H., Wouters, B.G., Knapp, M., Thibault, P., Laderoute, K., and Johnson, R.S. (2001). Transcription factor HIF-1 is a necessary mediator of the pasteur effect in mammalian cells. *Mol. Cell Biol.* 21, 3436–3444.
- Semenza, G.L. (2017). Hypoxia-inducible factors: coupling glucose metabolism and redox regulation with induction of the breast cancer stem cell phenotype. *EMBO J.* 36, 252–259.
- Takahashi, J.S. (2017). Transcriptional architecture of the mammalian circadian clock. *Nat. Rev. Genet.* 18, 164–179.
- Tarpey, M.D., Amorese, A.J., Balestrieri, N.P., Ryan, T.E., Schmidt, C.A., McClung, J.M., and Spangenburg, E.E. (2018). Characterization and utilization of the flexor digitorum brevis for assessing skeletal muscle function. *Skeletal Muscle* 8, 14.
- Terraneo, L., Virgili, E., Caretti, A., Bianciardi, P., and Samaja, M. (2014). In vivo hyperoxia induces hypoxia-inducible factor-1alpha overexpression in LNCaP tumors without affecting the tumor growth rate. *Int. J. Biochem. Cell Biol.* 51, 65–74.
- Terry, E.E., Zhang, X., Hoffmann, C., Hughes, L.D., Lewis, S.A., Li, J., Wallace, M.J., Riley, L.A., Douglas, C.M., Gutierrez-Monreal, M.A., et al. (2018). Transcriptional profiling reveals extraordinary diversity among skeletal muscle tissues. *Elife* 7, <https://doi.org/10.7554/eLife.34613>.
- Tian, Y.M., Yeoh, K.K., Lee, M.K., Eriksson, T., Kessler, B.M., Kramer, H.B., Edelmann, M.J., Willam, C., Pugh, C.W., Schofield, C.J., et al. (2011). Differential sensitivity of hypoxia inducible factor hydroxylation sites to hypoxia and hydroxylase inhibitors. *J. Biol. Chem.* 286, 13041–13051.
- Toledo, M., Batista-Gonzalez, A., Merheb, E., Aoun, M.L., Tarabra, E., Feng, D., Sarparanta, J., Merlo, P., Botre, F., Schwartz, G.J., et al. (2018). Autophagy regulates the liver clock and glucose metabolism by degrading CRY1. *Cell Metab.* 28, 268–281.e4.
- Ueda, H.R., Chen, W., Adachi, A., Wakamatsu, H., Hayashi, S., Takasugi, T., Nagano, M., Nakahama, K., Suzuki, Y., Sugano, S., et al. (2002). A transcription factor response element for gene expression during circadian night. *Nature* 418, 534–539.
- Vacanti, N.M., Divakaruni, A.S., Green, C.R., Parker, S.J., Henry, R.R., Ciaraldi, T.P., Murphy, A.N., and Metallo, C.M. (2014). Regulation of substrate utilization by the mitochondrial pyruvate carrier. *Mol. Cell* 56, 425–435.

Vitaterna, M.H., Selby, C.P., Todo, T., Niwa, H., Thompson, C., Fruechte, E.M., Hitomi, K., Thresher, R.J., Ishikawa, T., Miyazaki, J., et al. (1999). Differential regulation of mammalian period genes and circadian rhythmicity by cryptochromes 1 and 2. *Proc. Natl. Acad. Sci. U S A* 96, 12114–12119.

Wallace, M., Green, C.R., Roberts, L.S., Lee, Y.M., McCarville, J.L., Sanchez-Gurmaches, J., Meurs, N., Gengatharan, J.M., Hover, J.D., Phillips, S.A., et al. (2018). Enzyme promiscuity drives branched-chain fatty acid synthesis in adipose tissues. *Nat. Chem. Biol.* 14, 1021–1031.

Wu, D., Potluri, N., Lu, J., Kim, Y., and Rastinejad, F. (2015). Structural integration in hypoxia-inducible factors. *Nature* 524, 303–308.

Wu, D., and Rastinejad, F. (2017). Structural characterization of mammalian bHLH-PAS transcription factors. *Curr. Opin. Struct. Biol.* 43, 1–9.

Wu, D., Su, X., Potluri, N., Kim, Y., and Rastinejad, F. (2016). NPAS1-ARNT and NPAS3-ARNT crystal structures implicate the bHLH-PAS family as multi-ligand binding transcription factors. *Elife* 5, <https://doi.org/10.7554/eLife.18790>.

Wu, Y., Tang, D., Liu, N., Xiong, W., Huang, H., Li, Y., Ma, Z., Zhao, H., Chen, P., Qi, X., et al. (2017). Reciprocal regulation between the circadian clock and hypoxia signaling at the genome level in mammals. *Cell Metab.* 25, 73–85.

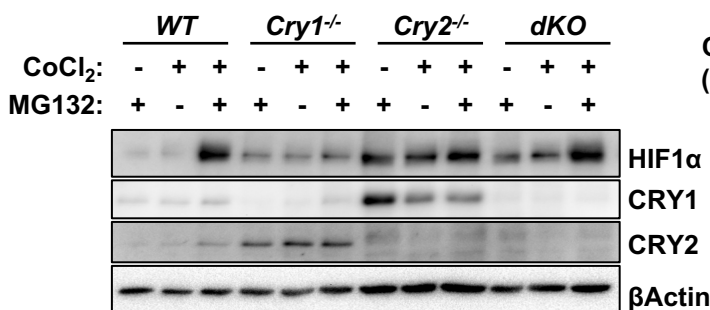
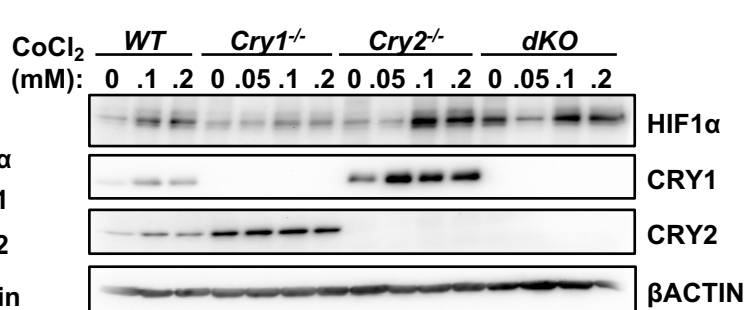
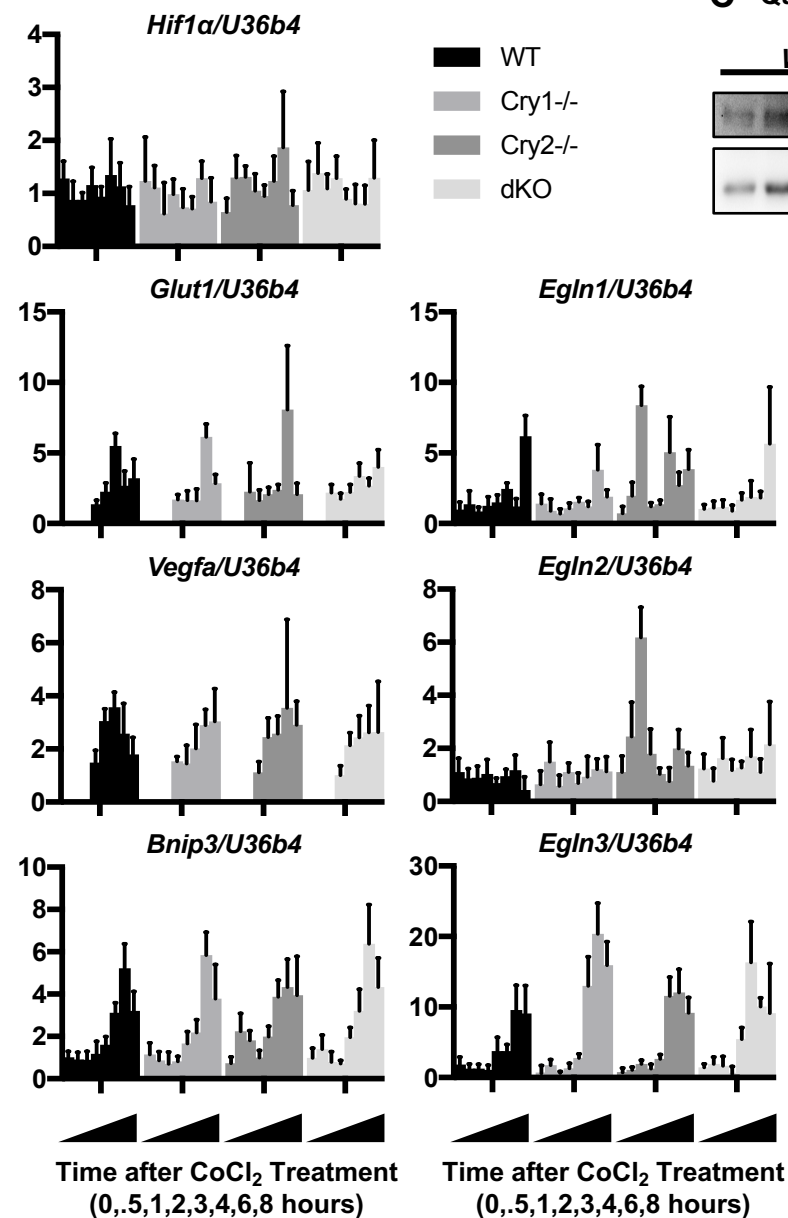
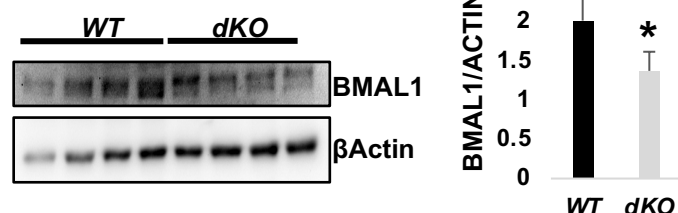
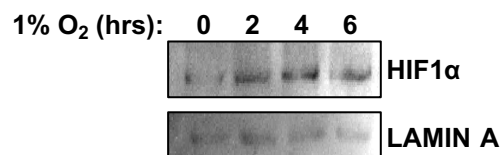
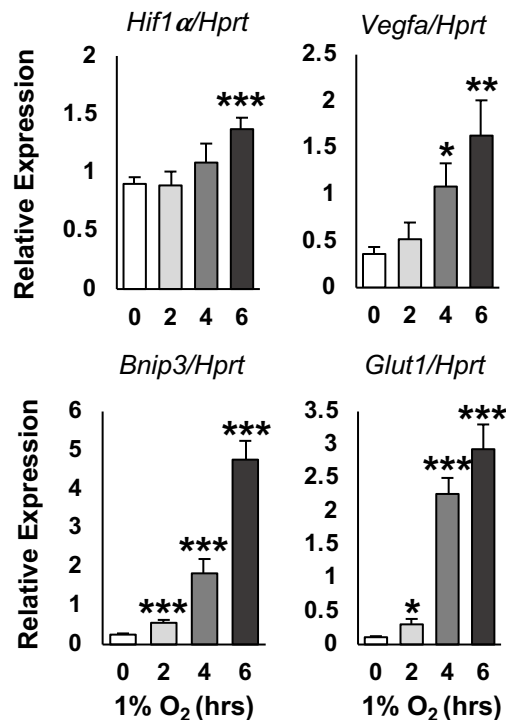
Yuan, Y., Hilliard, G., Ferguson, T., and Millhorn, D.E. (2003). Cobalt inhibits the interaction between hypoxia-inducible factor- α and von Hippel-Lindau protein by direct binding to hypoxia-inducible factor- α . *J. Biol. Chem.* 278, 15911–15916.

iScience, Volume 23

Supplemental Information

Cryptochromes Suppress HIF1 α in Muscles

Megan E. Vaughan, Martina Wallace, Michal K. Handzlik, Alanna B. Chan, Christian M. Metallo, and Katja A. Lamia

A Fibroblasts**B Fibroblasts****F Fibroblasts****C Quadriceps ZT14****D Myotubes****E****Figure S1: CRYs Suppress HIF1α. Related to Figure 1.**

(A,B) HIF1α, CRY1, CRY2, and βACTIN detected by IB in EFs isolated from mice of the indicated genotypes and treated with vehicle (-) or 100μM CoCl₂ (+, or as indicated) in the presence (+) or absence (-) of 20 μM MG132. (C) Endogenous BMAL1 detected by IB in nuclear extracts of quadriceps muscles of female mice dissected at ZT14. Quantification, right. * P < 0.05 by t-test. (D) HIF1α and LAMIN A detected by IB in WT 1°MTs exposed to 1% O₂ for 0-6 hours. (E) Expression of the indicated transcripts measured by quantitative PCR (qPCR) in 1°MTs plated and treated as in (D), normalized to *Hprt*. (F) Expression of the indicated transcripts measured by qPCR in EFs treated with 100μM CoCl₂ for 0-8 hours, normalized to *U36b4*.

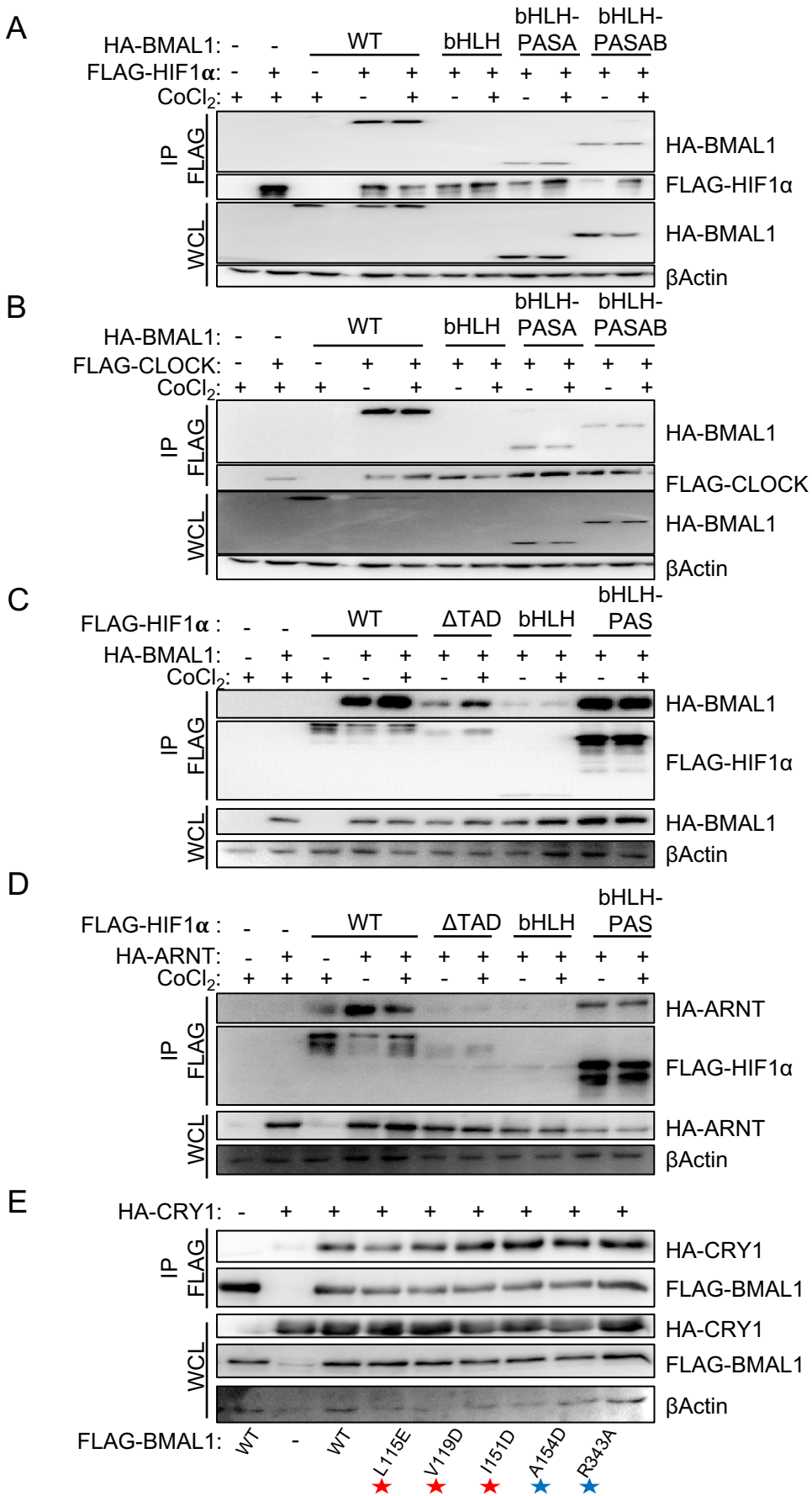


Figure S2: HIF1 α Interacts with Clock Proteins via Unique Domains. Related to Figure 3.

(A-E) Proteins detected by immunoblot (IB) following FLAG IP from lysates of HEK293T cells expressing the indicated plasmids and treated with either vehicle control or 100 μ M CoCl₂. Note that bHLH domains cannot be evaluated because we cannot detect them due to their small size.

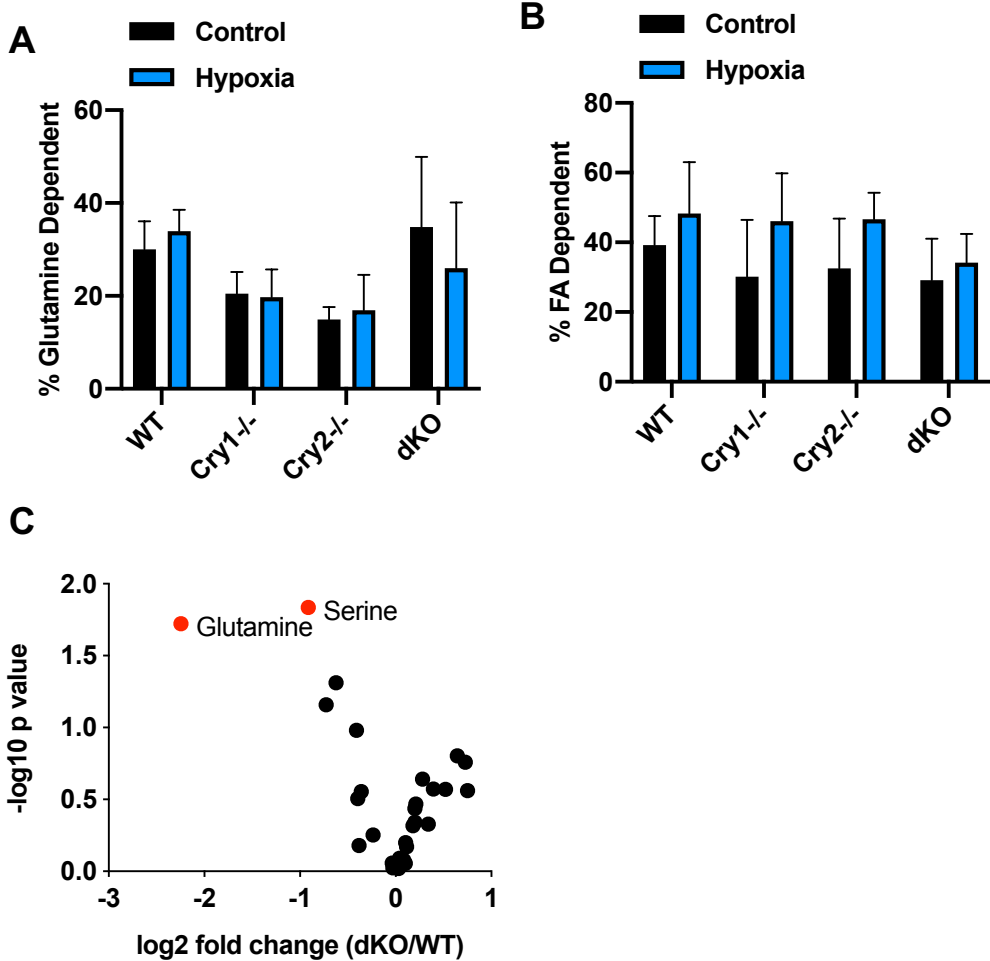


Figure S3: CRYs alter Muscle Metabolic Profile. Related to Figure 5.

(A,B) Glutamine (A) and fatty acid (B) dependency measured in 1°MTs isolated from mice of the indicated genotype and treated with either vehicle control or 100µM CoCl₂. (C) Metabolite abundance measured in quadriceps muscles from mice of the indicated genotypes.

TRANSPARENT METHODS

Contact for reagent and resource sharing

Further information and requests for reagents or resources should be directed to the Lead Contact, Katja Lamia (klamia@scripps.edu)

Mouse models: *dKO* mice were from Dr. Aziz Sancar (Thresher *et al.*, 1998). They were backcrossed ≥ 10 generations to c57Bl6/J prior to transfer to us and we performed an additional 4 backcrosses to c57Bl6/J mice from the TSRI breeding colony. Mice were maintained in standard 12:12 light:dark conditions and were given ad libitum access to normal chow and water. All animal care and treatments were in accordance with Scripps Research guidelines for the care and use of animals.

Cell lines: Primary myoblasts were isolated from six-week-old male *WT*, *Cry1^{-/-}*, *Cry2^{-/-}*, and *Cry1^{-/-};Cry2^{-/-}* (*dKO*) littermates. Isolation and culture conditions for myoblasts and myotubes are as previously described (Vaughan and Lamia, 2019). 293T (ATCC® CRL3216™) cells were purchased from the American Type Culture Collection (ATCC) and are derived from female human embryonic kidney cells. U2OS (ATCC® HTB-96™) cells were purchased from the American Type Culture Collection (ATCC) and are derived from female osteosarcoma cells. HEK293T cells were grown in complete Dulbecco's Modified Eagle's Medium (DMEM) (Invitrogen #10569) supplemented with 10% fetal bovine serum, and 1% penicillin and streptomycin. Ear fibroblasts (EFs) were isolated from six-week-old male *WT*, *Cry1KO*, *Cry2KO*, and *DKO* littermates. EFs were grown in complete Dulbecco's Modified Eagle's Medium (DMEM) supplemented with 15% fetal bovine serum, and 1% penicillin and streptomycin. Cells were grown in a 37°C incubator maintained at 5% CO₂.

Drug treatment: All CoCl₂ treatments were performed by dissolving Cobalt(II) chloride anhydrous crystals (Sigma #60818) in warm culture media at a concentration of 100 μ M. All treatments were performed for 4 hours prior to cell collection. DMOG and MG132 (Sigma C2211) were used at concentrations of 200 μ M and 20 μ M, respectively.

Cell culture and transfection: Transfections in HEK293T cells were performed using polyethylenimine (PEI; Polysciences Inc #23966-2) following standard protocols. pcDNA3-2xFlag-mCRY1 and pcDNA3-2xFlag-mCRY2 are described in (Lamia *et al.*, 2009). pBABE-mCRY2, pcDNA3-Myc-mCRY1, pcDNA3-Myc-mCRY2, pcDNA3-HA-mCRY1, pcDNA3-HA-mCRY2, and pcDNA3-2xFlag-Fbx13 are described in (Huber *et al.*, 2016). pcDNA3.1-HIF1 α -FLAG and pcDNA3.1-HIF1 β -HA were a gift from Dr. Carrie Partch. pLX304-HIF1 α -V5 was a gift from Dr. Enrique Saez. pcDNA3-2x-FLAG-BMAL1 and pcDNA3-2x-FLAG-CLOCK were a gift from Dr. Charles Weitz. All point mutations and truncations were generated using Q5 Site-Directed Mutagenesis kit and protocol (NEB #E0554S). pBABE-Puro was a gift from Dr. Tyler Jacks (MI, Boston, MA).

Co-immunoprecipitation and Western blotting: HEK293T whole cell extracts were prepared as previously described (Lamia *et al.*, 2009). Immunoprecipitation was performed using anti-Flag M2 agarose beads (Sigma #A2220) and anti-HA agarose beads (Sigma #A2095). Antibodies for Western Blots were anti-Flag polyclonal (Sigma #F7425), anti- β Actin (Sigma #A1978), anti-Cry1-CT and anti-Cry2-CT as described (Lamia *et al.*, 2011), anti-HIF1 α polyclonal (Novus Biologicals #NB100-449), anti-HIF1 β (Santa Cruz Biotechnology #sc-17811), anti-HA polyclonal (Sigma #H6908), anti-Myc Tag (Sigma #SAB1305535), and anti-Lamin A (Sigma #L1293).

Quantitative RT-PCR: RNA was extracted from EFs with Qiazol reagent using standard protocols (Qiagen #799306). cDNA was prepared using QScript cDNA Supermix (VWR #101414-106) and analyzed for gene expression using qPCR with iQ SYBR Green Supermix (Biorad #1708885). Primers used are listed in Table S1.

Nuclear Fractionation of Cells: Cells were washed with 5 mL cold PBS. 5 mL of fresh PBS was added before cells were scraped into falcon tubes and centrifuged for 5 minutes (2000 rpm). Cell pellets were transferred to 1.5-mL Eppendorf tubes and centrifuged 5 minutes (2000 rpm). Cell pellets were resuspended in Solution A (10 mM Hepes pH 8, 1.5 mM MgCl₂, 10 mM KCL, protease inhibitors, phosphatase inhibitors), and incubated for 15 minutes at 4 °C. An equal volume of Solution B was added (Solution A + 1% NP40) and incubated for an additional 5

minutes at 4 °C. Tubes were centrifuged for 5 minutes (3000 rpm). Cell pellets were washed twice with cold PBS and lysed in RIPA buffer.

Muscle Nuclear Fractionation: Quadriceps muscles were dissected from 8-week-old mice and then rinsed in cold PBS. Fractionation was performed as described (Dimauro *et al.*, 2012).

Luciferase Assays: U2OS cells were seeded at a density of 12,000 cells per 96-well. Cells were transfected after 24 hours with 35 ng reporter construct Per2Luc as described (Kriebs *et al.*, 2017), HRELuc (Addgene #26731, deposited by Dr. Navdeep Chandel), or pHIF1 α Luc (Addgene #40172, deposited by Dr. Alex Minella); 5 ng BMAL1; 15 ng CLOCK or HIF1 α ; 5 ng for ARNT; 2 ng Renilla Luciferase (a gift from Dr. Ian MacRae); 1-5 ng CRY1 or CRY2 or mCherry (as described in Kriebs *et al.* 2017). All plasmid dilutions were prepared fresh immediately before transfection. A media change was performed on the day following transfection. The following day luciferase activity was measured using the Dual-Glo[®] Luciferase Assay System (Promega #E2920).

Substrate Dependency Experiments: For Seahorse experiments (XF96, Seahorse Biosciences), XF96 plates were prepared as described (Vaughan *et al.* 2019). 3×10^4 primary myoblasts were seeded in 40 μ L of differentiation media in each well. Plated cells were grown in a chamber at 37 °C, 5% CO₂ for four days, during which time 80% of the media was replaced every day. OCR and ECAR were measured on day 5 following manufacturer's instructions in the Agilent Seahorse XF Mito Fuel Flex Test Kit (Agilent Technologies #103260-100). Data shown is a representative assay following three independent repeats of the fuel dependency test. Plate setup was varied between plates and wells on the perimeter of the plate were excluded from all experiments.

Hypoxia Experiments: For hypoxic chamber and hypoxia-mimicking drug treatment experiments, fibroblasts were plated at a density of 70-80% (~250,000 cells) on a 10-cm plate and left undisturbed for 24 hours after plating to allow attachment before exposure to hypoxia or CoCl₂. Myoblasts were plated in differentiation media and allowed to differentiate for 4 days, during which time the media was changed daily, prior to exposure to hypoxia or CoCl₂. Cell

plates were placed inside a 37°C incubator maintained at 1% O₂ for 0-6 hours prior to collection for 1% O₂ treatments. For experiments in which hypoxia was mimicked with drug treatments, the hypoxia-related exposure was induced by replacing the media with media containing 100 μM CoCl₂. For protein collection, nuclear fractionation was performed on 4-5 plates of cells in order to measure HIF1α levels. For qPCR analysis, RNA was collected from one plate of cells; all conditions were performed in triplicate.

Metabolic Tracing Experiments and Tissue Metabolite Analysis: Myotubes were seeded in differentiation media (Vaughan *et al.* 2019) at a density of 300,000 cells per well in six-well plates. Cells were allowed to attach to plates and differentiate for five days prior to isotope tracing when cells were incubated in media where the metabolite specified was replaced with the ¹³C labeled version for 24 hours. For cell culture and tissues, polar metabolites were extracted and analysed using GCMS as previously described (Wallace *et al.* 2018). The % isotopologue distribution of each metabolite was determined and corrected for natural abundance using in-house algorithms adapted from (Fernandez *et al.*, 1996). Mole percent enrichment (MPE) was calculated via the following equation:

$$\sum_{i=1}^n \frac{M_i \cdot i}{n}$$

where n is the number of carbon atoms in the metabolite and M_i is the relative abundance of the i th mass isotopologue.

Quantification and Statistical Analysis: Detailed descriptions of sample numbers and statistical tests are provided in the Figure Legends. In general, statistical analyses were done using two-tailed Student's t-test or with two-way ANOVA. Results presented are either a representative experiment or an average of three replicates ± SEM.

Data and Code Availability: This study did not generate or analyze any datasets or code.

KEY RESOURCES TABLE

REAGENT or RESOURCE	SOURCE	IDENTIFIER
Antibodies		
Anti-FLAG M2 agarose beads	Sigma	A2220
Anti-HA agarose beads	Sigma	A2095
Rabbit Anti-FLAG polyclonal	Sigma	F7425
Mouse Anti-Bactin	Sigma	A1978
Guinea pig Anti-Cry1-CT	Lamia et. al. 2011	N/A
Guinea pig Anti-Cry2-CT	Lamia et. al. 2011	N/A
Rabbit Anti-HIF1a polyclonal	Novus	NB100-449
Rabbit Anti-HIF1b	Santa Cruz Biotechnology	Sc-17811
Rabbit Anti-HA polyclonal	Sigma	H6908
Rabbit Anti-Myc tag	Sigma	SAB1305535
Rabbit Anti-PHD2	Novus Biologicals	NB100-2219
Rabbit Anti-LaminA	Sigma	L1293
Bacterial and Virus Strains		
psPAX	Addgene	12260
pMD2.G	Addgene	12259
pLKO.1 sh_Scramble	Addgene	1864
pBABE-Puro	Laboratory of Dr. Tyler Jacks	
Chemicals, Peptides, and Recombinant Proteins		
Cobalt Chloride Anhydrous	Sigma	60818
Polyethylenimine	Polysciences Inc	23966-2
MG132	Sigma	C2211
Critical Commercial Assays		
Q5 Site-Directed Mutagenesis Kit	NEB	E0554S
Qiazol	Qiagen	799306
Qscript cDNA Supermix	VWR	101414-106
iQ SYBR Green Supermix	Biorad	1708885
Dual-Glo Luciferase Assay System	Promega	E2920
Agilent Seahorse XF Mito Fuel Flex Test Kit	Agilent Technologies	103260-100
DMOG	Sigma	D3695
Experimental Models: Cell Lines		
Primary mouse ear fibroblasts and myotubes	This study	N/A
Human Embryonic Kidney 293T cells	ATCC	CRL3216
U-2 OS cells	ATCC	HTB-96
Experimental Models: Organisms/Strains		
<i>Cry1;Cry2</i> dKO mice	Thresher et. al. 1998	N/A
Oligonucleotides		
See Table S1	Table S1	Table S1
Recombinant DNA		
pcDNA3-2Xflag-mCRY1	Lamia et. al. 2009	N/A
pcDNA3-2xFlag-mCRY2	Lamia et. al. 2009	N/A
pBABE-mCRY2	Huber et. al. 2016	N/A

pcDNA3-Myc-mCRY1	Huber et. al. 2016	N/A
pcDNA3-Myc-mCRY2	Huber et. al. 2016	N/A
pcDNA3-HA-mCRY1	Huber et. al. 2016	N/A
pcDNA3-HA-mCRY2	Huber et. al. 2016	N/A
pcDNA3-2xFlag-Fbxl3	Huber et. al. 2016	N/A
pcDNA3.1-HIF1a-FLAG	Laboratory of Dr. Carrie Partch	N/A
pcDNA3.1-HIF1b-HA	Laboratory of Dr. Carrie Partch	N/A
pLX304-HIF1a-V5	Laboratory of Dr. Enrique Saez	N/A
pcDNA3-2x-FLAG-BMAL1	Laboratory of Dr. Charles Weitz	N/A
pcDNA3-2x-FLAG-CLOCK	Laboratory of Dr. Charles Weitz	N/A
pLKO.1 shRNA Fbxl3 #1	Sigma	TRCN0000126944
pLKO.1 shRNA VHL	Sigma	TRCN0000009737
Per2Luc	Kriebs et. al. 2017	N/A
pHIF1aLuc	Addgene	40172
HRELuc	Addgene	26731
pcDNA3-Renilla Luciferase	Laboratory of Dr. Ian MacRae	N/A
pcDNA3-mCherry	Kriebs et. al. 2017	N/A
Other		
Single Flow Meter	Stemcell Technologies	27311
Microplate Reader	Versamax	N/A